AWARD NUMBER: W81XWH-16-1-0503

TITLE: A Closed-Loop Neural Prosthesis for Restoration of Function after Traumatic Brain Injury

PRINCIPAL INVESTIGATOR: Pedram Mohseni, PhD

CONTRACTING ORGANIZATION: Case Western Reserve University, Cleveland, OH

REPORT DATE: December 2020

TYPE OF REPORT: Final

PREPARED FOR: U.S. Army Medical Research and Materiel Command
Fort Detrick, Maryland 21702-5012

REPORT DOCUMENTATION PAGE

Form Approved
OMB No. 0704-0188

1. REPORT DATE *(DD-MM-YYYY)*	**2. REPORT TYPE**	**3. DATES COVERED** *(From - To)*
December 2020	Final	01Sep2016 – 31Aug2020

4. TITLE AND SUBTITLE

A Closed-Loop Neural Prosthesis for Restoration of Function after Traumatic Brain Injury

5a. CONTRACT NUMBER

5b. GRANT NUMBER
W81XWH-16-1-0503

5c. PROGRAM ELEMENT NUMBER

6. AUTHOR(S)

Pedram Mohseni, Randolph J. Nudo, David J. Guggenmos

5d. PROJECT NUMBER

5e. TASK NUMBER

5f. WORK UNIT NUMBER

7. PERFORMING ORGANIZATION NAME(S) AND ADDRESS(ES)

Case Western Reserve University
10900 Euclid Avenue
Cleveland, OH 44106

Univ. of Kansas Medical Center Research
3901 Rainbow Boulevard, MSN 1039
Kansas City, KS 66103

8. PERFORMING ORGANIZATION REPORT NUMBER

9. SPONSORING / MONITORING AGENCY NAME(S) AND ADDRESS(ES)

U.S. Army Medical Research and Materiel Command
Fort Detrick, Maryland 21702-5012

10. SPONSOR/MONITOR'S ACRONYM(S)

11. SPONSOR/MONITOR'S REPORT NUMBER(S)

12. DISTRIBUTION / AVAILABILITY STATEMENT

Approved for Public Release; distribution unlimited

13. SUPPLEMENTARY NOTES

14. ABSTRACT

We successfully completed the rodent aims and demonstrated that activity-dependent stimulation (ADS) was effective even when treatment was delayed up to 3 weeks post-injury. With the one-week post-injury initiation, 4 weeks of treatment resulted in recovery of motor performance that persisted for 8 weeks, the total duration of the follow-up period. Moreover, we were able to develop a fully assembled and packaged nonhuman primate (NHP) microdevice that was small enough to be housed within a chronic, skull-affixed, primate chamber. Over a 2-week monitoring period, the NHP microdevice remained fully functional in a simulated *in vivo* environment with elevated humidity and temperature. Finally, we were able to demonstrate the first NHP model of controlled cortical impact (CCI) injury designed for long-term behavioral assessment. We established procedures for implantation of the NHP microdevice within a chronic chamber and for microelectrodes implantation in target cortical locations. We also demonstrated that we could perform spike-triggered stimulation reliably in a squirrel monkey. We are now in an excellent position to test the ability of ADS to enhance behavioral recovery after such injuries.

15. SUBJECT TERMS
Activity-dependent stimulation; Implantable microsystem; Neuroplasticity; Rehabilitation, Traumatic brain injury

16. SECURITY CLASSIFICATION OF:			**17. LIMITATION OF ABSTRACT**	**18. NUMBER OF PAGES**	**19a. NAME OF RESPONSIBLE PERSON**
a. REPORT	**b. ABSTRACT**	**c. THIS PAGE**			USAMRMC
U	U	U	UU	78	**19b. TELEPHONE NUMBER** *(include area code)*

TABLE OF CONTENTS

1. INTRODUCTION:

The goal of this project is to use an implantable brain-machine-brain interface (BMBI) to facilitate functional reorganization in spared cortico-cortical connections and enhance behavioral recovery after traumatic brain injury (TBI) in both rodent and non-human primate (NHP) models, which will remarkably advance the neurorehabilitation field at the level of functional neurons and networks.

2. KEYWORDS:

Activity-dependent stimulation; Implantable microsystem; Neuroplasticity; Rehabilitation; Traumatic brain injury

3. ACCOMPLISHMENTS:

What were the major goals of the project?

Major Task 1: Develop functional microdevices for rodent studies for Aim 1 – Completed
Major Task 2: Conduct preclinical efficacy study for optimal time window in ambulatory rats using rodent microdevice – Completed
Major Task 3: Develop functional microdevices for rodent studies in Aim 2 – Completed
Major Task 4: Conduct preclinical efficacy study for persistence of therapeutic effects in ambulatory rats using rodent microdevice – Completed
Major Task 5: Develop functional microdevices for non-human primate studies – Completed
Major Task 6: Conduct preclinical efficacy study in ambulatory non-human primates – 50% Completed

What was accomplished under these goals?

In this section of the final report, we describe the research accomplishments associated with each Major Task of the project as listed in the approved Statement of Work.

Specific Aim 1 – Determine the optimal post-injury time window to apply ADS treatment

Major Task 1: Develop functional microdevices for rodent studies for Aim 1

Subtask 1: Electronics development and testing: Our activity-dependent stimulation (ADS) application-specific integrated circuit (ASIC) featuring two identical 4-channel modules was successfully submitted to The MOSIS Services in April 2017 for re-fabrication using AMS 0.35 µm 2P/4M CMOS. The ASIC incorporated a fully integrated neural recording front-end comprising a low-noise two-stage amplification circuitry and a 10-bit successive approximation register (SAR)-based analog-to-digital converter (ADC). The ac-coupled amplification circuitry could provide a maximum mid-band ac gain of ~66 dB at 1 kHz with a measured input-referred noise voltage of ~3.1 μV_{rms} from 0.5 Hz to 50 kHz, while dissipating ~27 µW from 1.5 V. The ADC featured an effective number of bits (ENOB) of 9.2 for sampling frequency of 35.7 kSa/s, while dissipating only 6 µW. The ASIC also incorporated monolithic circuitry to identify the presence of large action potentials in the recorded digitized data with a spike discrimination algorithm based on two programmable threshold levels and time-amplitude windows. A first-order, digital, highpass filter removed any dc/low-frequency artifacts prior to spike discrimination. The power consumption per channel was less than 1 µW with a 1.5 V supply and ADC sampling frequency of 35.7 kSa/s.

The ASIC featured decision-making circuitry implemented as a programmable gate array to provide any logic combination of four spike discriminator outputs as a trigger signal for stimulation activation using a 16b combination code for each stimulation channel. A high-output-impedance current microstimulator could deliver a maximum current of 94.5 µA (6b-programmable) to the target cortical tissue with current efficiency of 95.6% and voltage compliance of 4.68 V (from 5-V supply), when configured for monophasic stimulation with passive discharge. Finally, the ASIC incorporated a highly integrated voltage converter to generate 5-V supply for the stimulus back-end from a miniature primary battery (1.5 V) that powered the entire system. The voltage converter employed only one external capacitor (1 µF) for storage, and delivered a maximum dc load current of ~88 µA with power efficiency of 31% with its output voltage adjusted to 5.05 V. The re-fabricated chips were received from MOSIS in July 2017. Upon benchtop testing of them, the electronic design was proved fully functional as before (Azin, et al., 2011a).

Subtask 2: Microdevice assembly and testing: Miniature rigid-flex substrates were fabricated through Flexible Circuit Technologies (Plymouth, MN). The ASIC that was developed in **Subtask 1** was assembled on the 4-layer substrate made from FR-4 (rigid) and polyimide (flexible) sections, together with various other components. We worked with ProtoConnect (Ann Arbor, MI) for die attachment, encapsulation, wire bonding, and assembly of all the components onto the substrate. The microdevice was designed to connect to two chronically implanted recording and stimulating microelectrodes (NeuroNexus Technologies, Ann Arbor, MI) via two microconnectors (Omnetics Corp., Minneapolis, MN) in plug-and-play fashion. **Figure 1** depicts the schematic block diagram and a photograph of the fully assembled microdevice. In parallel, significant work was also performed in collaboration with the neurobiology team at KUMC to successfully upgrade the hardware and software platforms in the

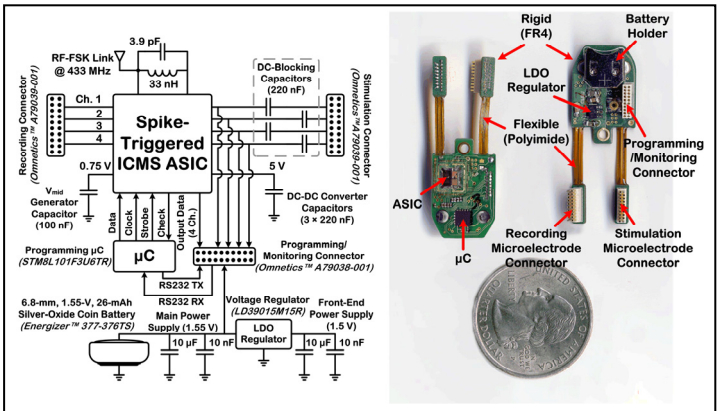

Figure 1: *Schematic block diagram and a photograph of the fully assembled microdevice for activity-dependent intracortical microstimulation in an ambulatory rat (Azin, et al., 2011b).*

extant experimental setup at KUMC for compatibility with new computers and operating systems. This effort allowed the KUMC team to proceed with validating the functionality of several existing rodent microdevices for performing animal studies, while new microdevices were being re-developed.

Major Task 2: Conduct preclinical efficacy study for optimal time window in ambulatory rats using rodent microdevice

Subtask 1: Complete institutional IACUC and ACURO review process: An animal care and use protocol was submitted to the KUMC IACUC on 03/02/2017. Upon approval, we submitted the protocol to ACURO on 04/14/2017. We received approval from ACURO on 08/23/2017, permitting initiation of **Major Task 2**. Thus, **Subtask 1** milestone (i.e., obtain approval for animal protocol) was achieved on 08/23/2017, covering the animal care and use for all the specific aims.

Subtask 2: Conduct ambulatory experiments for optimal time window (Aim 1): *Rationale:* In our previous DoD-funded studies, we demonstrated that ADS initiated immediately after TBI in rats resulted in rapid recovery of motor performance compared with open-loop stimulation or non-stimulated controls. This initial proof-of-principle study provided support for the current study to determine whether the treatment window could be expanded to a more clinically relevant timeframe. Because invasive treatments are less likely to be implemented immediately following brain injury, it was necessary to test if our treatments would be equally effective if implemented a week or more after injury. Rats were used for this aim, because a large database exists for TBI in this species including all of our work using the ADS approach to date. This allows comparisons with previous data. Rats are also the least sentient species that is suitable for the proposed study.

Study design: The main endpoint of this Aim consisted of behavioral recovery profiles on a skilled forelimb reaching task. This task consisted of rats reaching with the preferred forelimb to retrieve a food pellet located outside of the testing chamber, as described in our previous studies (Guggenmos, et al., 2013). For inclusion into the study, rats were required to perform successful retrievals on >70% of trials for three consecutive sessions. Rats entering the study were randomly assigned to one of four groups. In each of the four groups, rats received a controlled cortical impact (CCI) injury of the primary motor cortex caudal forelimb area (CFA), followed by implantation of the microdevice. All rats had identical care and post-surgical treatment for the first week post-injury. Rats in the three treatment groups underwent ADS via the microdevice for four weeks, initiated at 1, 2, or 3 weeks, respectively. In a fourth group, the microdevice remained inactive throughout the study, serving as a control group. In the three treatment groups, ADS was performed daily, while behavioral assessment was performed weekly with ADS turned on. After the 4-week ADS period, behavioral assessment was performed for one additional week. Following completion of the first cohort, a second cohort underwent the same procedures until the required number of rats completed the study.

Implant procedures: Details of the microdevice implantation procedure can be found in our previous publication (Guggenmos, et al., 2013; **Fig. 2**). Following neurophysiological identification of somatosensory and motor areas of interest, a CCI was delivered (3-mm tip diameter, 2-mm depth, 1.5-m/s velocity, 200-μs dwell time) to induce TBI. Two Michigan-style planar microelectrode arrays were implanted to interface the cortical tissue with the microdevice as described in our previous publication (Guggenmos, et al., 2013; **Fig. 3**). Following the implantation procedure, the skin was sutured and the microdevice was attached to the mounting post and connected to the electrode connectors (**Fig. 4**).

Microdevice operation: Microdevice functionality and quality of neural signals were monitored daily to ensure successful operation. On treatment days, the microdevice was configured to perform ADS. On Days 3, 5 and 7, behavioral assessments on the reaching task were performed. The microdevice was programmed to deliver a single 60-μA, 200-μs, monophasic pulse into the S1 forelimb area 7.5 ms after detection of an extracellular neural action potential in the RFA (**Fig. 5**). This was followed by 20.5-ms blanking period in which spikes could be detected but would not trigger stimulation. Once configured, ADS was run continuously for four weeks, except during battery replacement and signal checks.

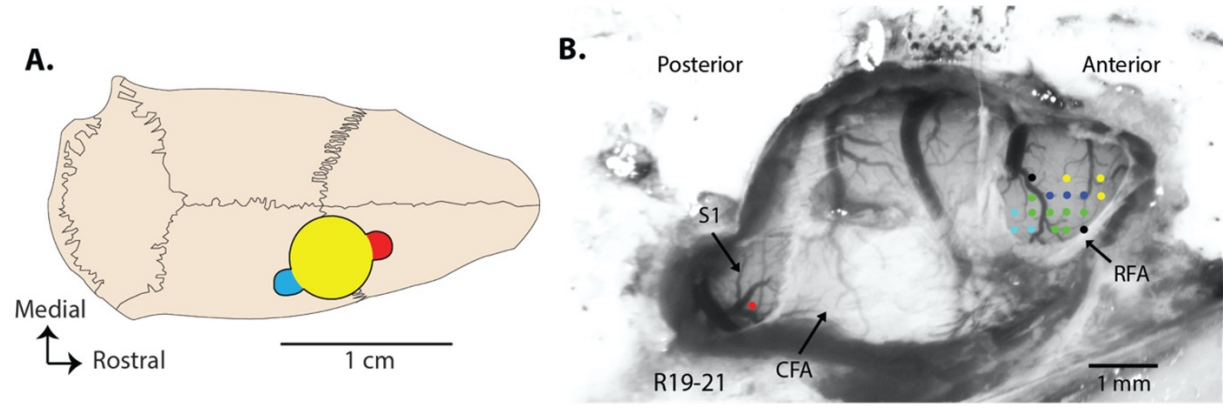

Figure 2: *Identification of regions of interest in cerebral cortex.* ***A.*** *General location of craniectomy, including a burr hole located over the caudal forelimb area (CFA; yellow), rostral extension of opening to expose the rostral forelimb area (RFA; red), and caudal extension of opening to expose the somatosensory (S1) forelimb area (blue).* ***B.*** *Photograph of cortical surface showing locations of RFA and S1 forelimb area verified by intracortical microstimulation and multi-unit extracellular recording techniques, respectively. To perform neurophysiological identification, it was necessary to remove the dura over target locations.*

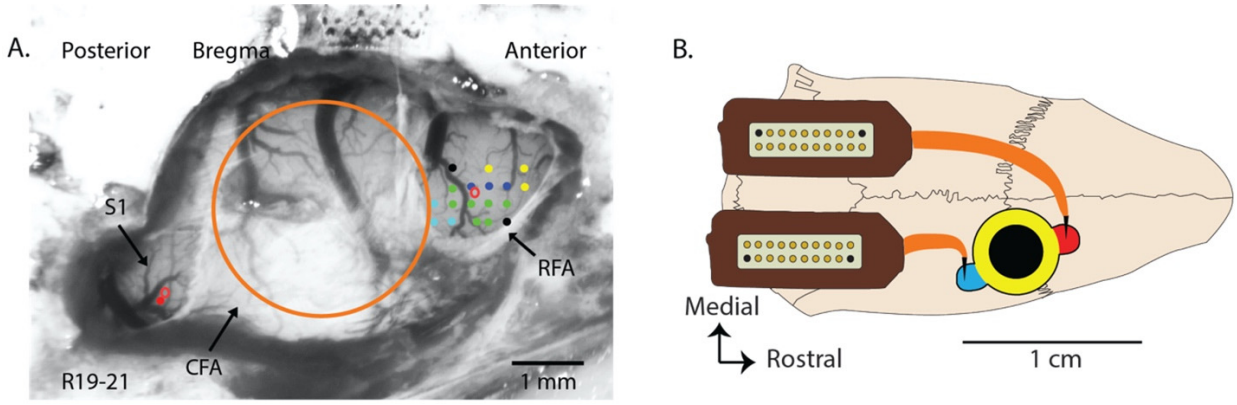

Figure 3: *Overview of microdevice implantation.* ***A.*** *Photograph of cortical surface showing locations of RFA and S1 forelimb area verified by intracortical microstimulation and multi-unit extracellular recording techniques, respectively (same as Fig. 2B).* ***B.*** *Location of microelectrode arrays in RFA and S1 and array connectors over the posterior aspect of the skull.*

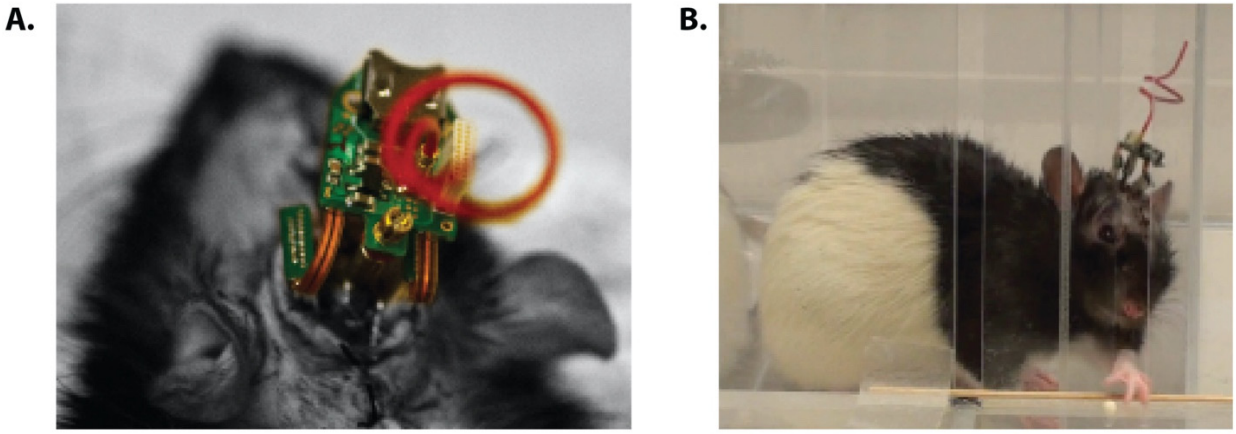

Figure 4: *Rat with microdevice attached.* ***A.*** *Microdevice affixed to rat skull.* ***B.*** *Rat performing pellet retrieval task used as primary outcome measure in the study. The red wire served as an antenna for wireless operation.*

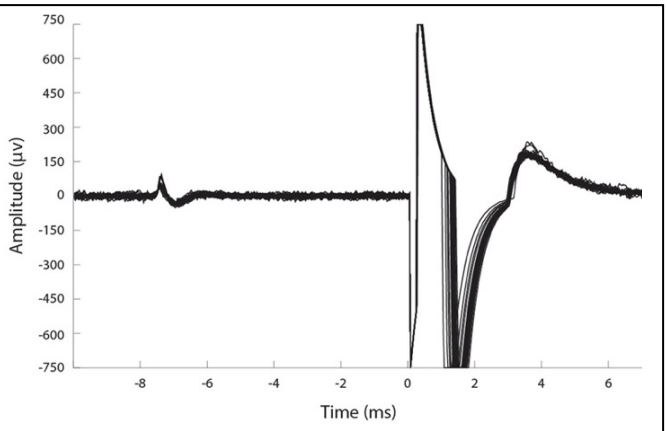

Figure 5: *Typical recording of neural spikes detected in RFA in a rat performing the pellet-retrieval task. Several traces are superimposed. Detected neural spikes are shown at ~ -7.5 ms. Stimulus artifact from stimulation pulse in S1 is shown beginning at ~ 0 ms.*

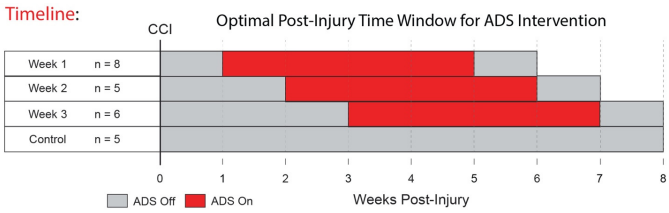

Figure 6: *Experimental timeline (Aim 1).*

The control group underwent the same procedures, but the stimulation was never activated. For all conditions, task performance was assessed prior to, during, and one week following the cessation of stimulation. For the control group, this behavior was monitored for eight total weeks (matching the total duration of recording as the Wk 3 group). A summary of the experimental timeline is shown in **Fig. 6**.

Statistical analyses: Behavioral data were analyzed using a generalized linear mixed model with a restricted maximum likelihood estimation to examine the stimulation effect on recovery of motor performance. Models were adjusted for the fixed effects of stimulation status and time, in addition to the interaction of time with stimulation status, group, and both stimulation status and group (three-way interaction). Linear contrasts were used to estimate the slopes of recovery, slope post-stimulus, and the difference in scores post-stimulus.

Behavioral results: The primary endpoint for Aim 1 was motor performance on the reaching task after treatment. Behavioral performance in each of the three treatment groups compared with the control group is shown in **Fig. 7**. We found a significant difference among all groups ($p < 0.0001$). Pair-wise comparisons showed no significant difference between the treatment groups (1 Wk, 2 Wk, and 3 Wk delays) ($p = 0.0591$), but significant differences between all treatment groups and the controls. The secondary endpoint was the slope of recovery profile *while the stimulation was on*. We found a significant effect ($p = 0.0004$), with pair-wise comparisons indicating both Wk 1 and Wk 2 delays having a significantly different slope than Wk 3 delay ($p = 0.0001$ and $p = 0.0319$, respectively). Furthermore, we tested whether there was an overall difference in slope *over the entire duration of the study*. This was also significant ($p < 0.0001$), with the Wk 1 delay showing the only pair-wise difference to control ($p = 0.0083$). This is likely due to a combination of treatment delay and spontaneous recovery.

Histological results: To maximize the data collected from these animals, we are also analyzing axonal projections from RFA to other cortical regions (specifically S1, the target of our stimulation) using the neuronal tract-tracer biotinylated dextran amine (BDA). This analysis may allow us to determine structural changes that might take place because of ADS.

Discussion and conclusions: Our previous findings from prior DoD-funded work demonstrated efficacy for ADS treatment in a rat CCI model of TBI (Guggenmos, et al., 2013). In these prior studies, the ADS treatment was initiated very early (within one day) after the injury. While this result provided proof-of-principle for ADS as a potential treatment, implantation of a device within this timeframe was not considered clinically feasible. It was highly desirable to extend the window for effective treatment to account for the time required for TBI patients to be transported to a surgical facility and to allow for the patients to be medically stabilized. Since post-injury edema often occurs within the first week in such patients, we sought to determine if the treatment was efficacious when delayed at least one week.

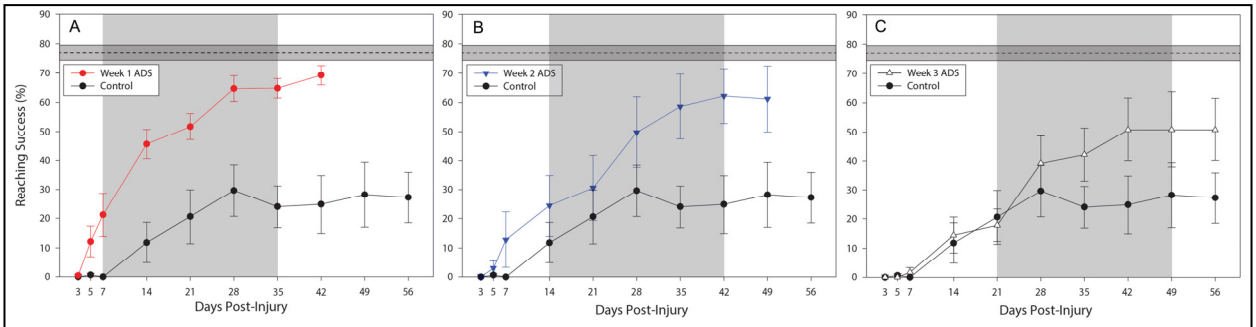

Figure 7: *Effects of delaying ADS initiation on motor performance.* ***A.*** *ADS initiated 1 week after TBI.* ***B.*** *ADS initiated 2 weeks after TBI.* ***C.*** *ADS initiated 3 weeks after TBI. Treatment period is shown in shaded area.*

The results demonstrated a significant benefit of four weeks of ADS treatment compared with untreated controls, even when initiated at post-injury delays of 1, 2 or 3 weeks. Even with the longest delay of 3 weeks, the effects of the treatment could be seen within one to two weeks of treatment initiation, with motor performance continuing to improve with further treatment (**Fig. 7**). Qualitatively, it is noteworthy that the final motor performance was best with a delay of 1 week, with rats achieving reaching success nearly equivalent to baseline performance (red line in **Fig. 7A**). Final motor performance was a bit less in the 2-week delay group (blue line in **Fig. 7B**) and even less in the 3-week delay group (grey line in **Fig. 7C**), but all groups were significantly better than untreated controls. As noted above, the slopes in the 1- and 2-week groups were significantly different from that of the 3-week group. This study further supports the use of ADS to treat motor deficits after TBI and demonstrates that this invasive approach can be used in a clinically relevant timeframe. While the results suggest that treatment should be initiated as soon as possible after injury, efficacy was shown with a delay of up to 3 weeks, allowing ample time in a clinical setting for resolution of edema and to assure that the patient is medically stable for a neurosurgical procedure to introduce microelectrodes into the cortex and attach the microdevice to the skull.

Current status: We published an abstract and presented a poster describing the behavioral results of Aim 1 at the 2019 Society for Neuroscience Annual Meeting (Hudson, et al., 2019). We anticipate submitting a manuscript for publication within 3 months.

Specific Aim 2 – Determine the time course for persistence of ADS treatment effects

Major Task 3: Develop functional microdevices for rodent studies in Aim 2

Subtask 1: Microdevice assembly and testing: The CWRU team delivered functional rodent microdevices to the KUMC team at a sufficient quantity to perform both Aims 1 and 2 of the project.

Major Task 4: Conduct preclinical efficacy study for persistence of therapeutic effects in ambulatory rats using rodent microdevice

Subtask 1: Complete institutional IACUC and ACURO review process: This milestone (i.e., obtain approval for animal protocol) was achieved on 08/23/2017, covering the animal care and use for all the specific aims.

Subtask 2: Conduct ambulatory experiments for persistence of therapeutic effects (Aim 2): *Rationale:* Aim 2 was designed to determine if the effects of ADS persisted following cessation of the stimulation therapy. Along with the effects of time after injury that were tested in Aim 1, determination of persistence in a preclinical model was considered to be critical prior to pursuing this approach in a non-human primate (NHP) model, and eventually in clinical cohorts. It would be highly desirable to have a device that would be effective using short-term (up to 1 month) treatment and that could be explanted following treatment. If chronic implantation were required, clinical feasibility would be compromised, since risk of infection would increase. Also, the typically short (weeks to months) lifespan of reliable spike recordings might hinder the usability of the device to a narrow window. Thus, Aim 2 was designed

to examine the persistence of treatment effects after the device was turned off. A secondary goal was to test the duration of ADS treatment required for persistent benefit.

Study design: The original experimental design called for four groups varying in treatment duration (4 weeks, 6 weeks, 8 weeks, and control) that would examine whether the duration of treatment would also impact the persistence of the behavioral recovery effects. However, due to the limited supply of ASICs, we chose to first complete the shortest treatment duration (4 weeks) compared to untreated control animals. The rationale for this was that if the shortest treatment period showed persistent benefits for motor performance, there was not a compelling need to test therapeutic sessions of longer duration. Therefore, we initially tested two groups, a treatment group with ADS therapy initiated at one week post-injury and continuing for 4 weeks and a control group receiving no stimulation. Following the 4-week treatment period, behavioral assessments were continued for 13 weeks post-lesion (8 weeks post-treatment) to examine persistence. The primary question to be answered in this aim was "is there a decrement in performance from the end of treatment to the end of the study, and if so what is the rate of this decline?" All procedures were identical to those described above for Aim 1. Further details can be found in Guggenmos, et al., 2013. The experimental timeline is shown in **Fig. 8**.

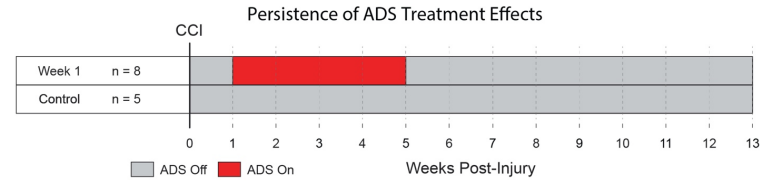

Figure 8: *Experimental timeline (Aim 2).*

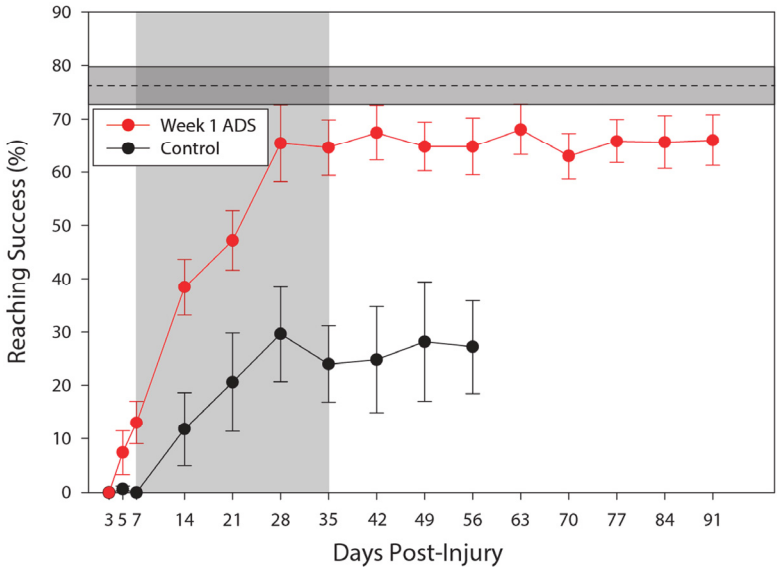

Figure 9: *Persistence of effects of ADS treatment. Treatment period is shown in shaded area.*

Behavioral results: The primary endpoint for Aim 2 was whether there was a post-treatment decline in motor performance in the 8-week period following cessation of stimulation. We found no significant difference between the calculated slope (-0.00554) and 0 ($p = 0.96$), indicating no longitudinal change in performance after stimulation was terminated. Thus, as illustrated in **Fig. 9**, during the 4-week course of ADS treatment, motor performance recovered to near baseline levels after three weeks, and this improved performance persisted after treatment without decrement.

Electrophysiological results: We extracted multi-unit spiking data, discriminated stimulus-triggering neuronal data, and stimulation data from all behavioral testing days. We did not find any significant longitudinal changes in mean firing rate or in mean stimulation rate across sessions or groups. Further analysis is underway to determine if there were any differences in the evoked response to stimulation.

Discussion and conclusions: Taken together with the results from Aim 1, these results indicate that ADS therapy is effective in restoring behavioral performance on a reaching task in a rat model of TBI even if the treatment is delayed up to 3 weeks post-injury. Furthermore, at least with a delay in treatment initiation of one week post-injury, the benefits of four weeks of ADS persist for at least eight weeks after treatment ends. These results strengthen the clinical viability of ADS as a treatment for TBI since we have

demonstrated that treatment can be delayed after the acute injury for up to three weeks and that the effects persist after termination of the treatment.

Current status: The behavioral portion of the study is complete. Following completion of histological analyses, we will submit a manuscript for publication. We anticipate submission within 3 months.

Specific Aim 3 – Determine the efficacy of the neural prosthesis in a nonhuman primate model of TBI

Major Task 5: Develop functional microdevices for non-human primate studies

Subtask 1: Microdevice assembly and testing: The next step in the evolution of our ADS treatment approach was to demonstrate its efficacy in driving motor function recovery in an NHP model of TBI. However, such an effort was generally hindered by the lack of a bidirectional wireless communication link between the microdevice and a user base station (UBS). Specifically, while the ASIC did incorporate a radio-frequency frequency-shift-keyed (RF-FSK) transmitter operating at ~433 MHz for wirelessly transmitting the neural activity on a selected channel to the UBS via the uplink, programming various ASIC parameters or temporarily monitoring its operation could only be done via a wired link from the UBS. While this strategy was feasible in rodent experiments, due to the ease of accessing the head-mounted system for connecting the wired link on a temporary basis, this approach would not work well in experiments with NHPs in which the head-mounted system is typically enclosed within a skull-affixed primate chamber, making it impractical to use a wired link for programming the ASIC or monitoring its function during longitudinal studies.

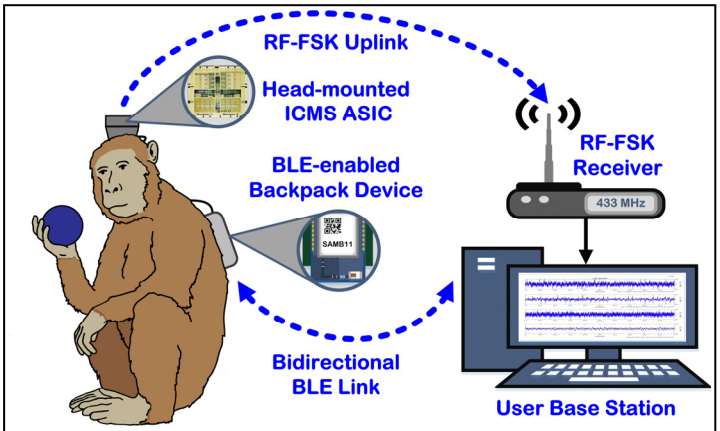

Figure 10: *Illustration of an experimental setup involving a non-human primate equipped with BLE-enabled backpack device for bidirectional wireless communications b/w head-mounted neural microdevice and user base station.*

Bidirectional wireless link development: We set out to address this limitation by developing a low-power, bidirectional, wireless communication link between the head-mounted ASIC and the UBS using Bluetooth low energy (BLE), an emerging technology for biomedical applications. **Figure 10** illustrates an experimental setup involving an NHP equipped with the ASIC as part of a head-mounted device enclosed within a primate chamber, as well as a backpack device that contains a BLE module for bidirectional wireless communications with the UBS.

Figure 11 depicts the system architecture for the implementation of the BLE-enabled, bidirectional, wireless communication link with the ASIC. The system can be partitioned into three separate sub-systems, namely, a UBS, a BLE module (SAMB11, *Atmel*) and power supply management electronics that are housed in the backpack device, and the ASIC and a microcontroller unit (MCU, STM8L151G6U6, *STMicroelectronics*) that are housed in the head-mounted device. The UBS hosts a BLE user interface that is custom developed in C# for a Windows-based operating system (OS). This interface serves as a client-side console through which the user can initiate various BLE tasks for bidirectional communications with the ASIC using a universal serial bus BLE dongle (BlueGiga BLED112, *Silicon Labs*). Moreover, the UBS houses a LabVIEW-based platform to receive and process neural signals recorded on one ASIC channel through the RF-FSK uplink at ~433 MHz that is integrated onto the ASIC.

The backpack device contains the BLE module, which serves as an intermediary data server between the UBS and the ASIC. Various tasks that require communications with the ASIC are commanded by the SAMB11 BLE module to the MCU via a universal asynchronous receiver-transmitter (UART) bus after

bidirectional level shifting between 3.6 V and 1.8 V. The backpack device also contains the power supply-management electronics, including a lithium-ion battery that directly powers the BLE module and a 1.8-V buck converter that powers the low-power MCU. The buck converter also powers two low-drop-out (LDO) regulators that generate the 1.5-V analog and digital supplies of the ASIC. A resistive voltage divider generates a reference voltage, V_{MID}, which is used for power supply level monitoring via the SAMB11 BLE module. Finally, the head-mounted device contains the ASIC, low-power MCU, and the two LDOs for generating the ASIC power supplies. Utilizing the bidirectional nature of the BLE link, the system is designed to feature stimulus rate and site impedance monitoring for reporting back to the UBS upon user demand.

Figure 12 illustrates the communication flow between the BLE user interface of the UBS and the ASIC for both programming and monitoring purposes. For all operations, the data received by the SAMB11 BLE module are stored within custom generic-attribute (GATT) characteristics. For ASIC programming purposes, 95 bytes of data are generated on the UBS and transmitted to the BLE module, containing the settings for the analog and digital blocks of the ASIC (92 bytes), as well as the setting for the source of stimulus trigger (3 bytes). The trigger source can be derived either in an activity-dependent manner from the ASIC itself (closed-loop) or via a *Trigger* signal from the MCU (open-loop). A simple checksum routine is preformed when the programming data are received by the MCU. If valid, the MCU will configure the trigger source and program the ASIC via the programming interface comprised of *Clock*, *Data*, and *Strobe* signals. In return, the ASIC sends back to the MCU an acknowledgment via a *Check* signal as the programming status, which is subsequently transmitted to the BLE module for notifying the UBS. If programming is successful, the MCU will save the programming data to its EEPROM for ASIC boot-up programming. Otherwise, the UBS is notified of the failure, and the MCU will skip over the EEPROM routine.

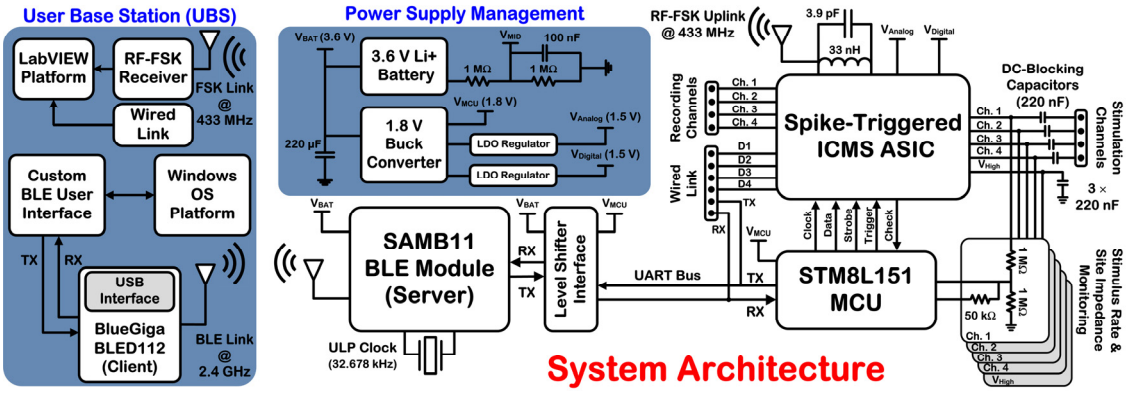

Figure 11: *System architecture for the implementation of a BLE-enabled, bidirectional, wireless communication link between the ASIC and the user base station.*

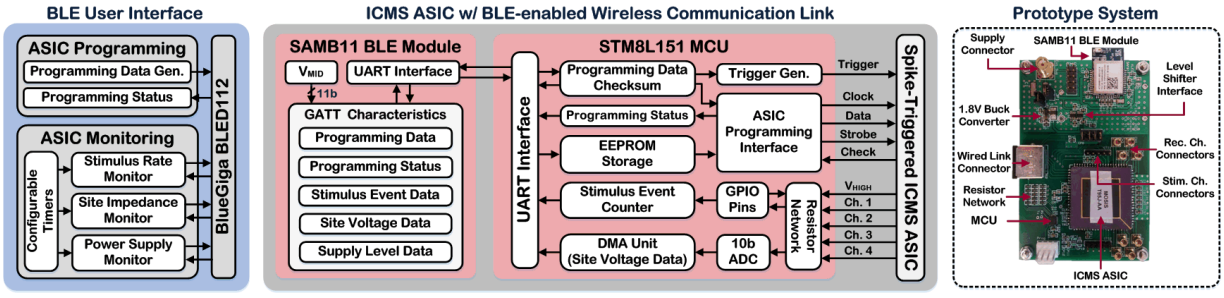

Figure 12: ***Left*** *– Illustration of the communication flow between the custom BLE user interface in the user base station and the ASIC.* ***Right*** *– Photograph of the system prototype, incorporating the ASIC, SAMB11 BLE module, and all requisite peripheral hardware.*

For ASIC monitoring purposes, the UBS receives information such as the average stimulus rate, electrode site impedance, and power supply level. These monitors can be set to execute on command or poll periodically by utilizing configurable timers located on the UBS. Specifically, the average stimulus rate per channel is monitored by counting the number of stimulation events within a pre-specified time window tracked by the UBS timers. The electrode site impedance is monitored by recording the corresponding site voltage waveform (and that of the "high" voltage output of the ASIC) using the 10b ADC of the MCU and transmitting the information to the UBS via the BLE module. A custom script on the UBS next analyzes the waveforms to evaluate the level of the site impedance. Finally, the supply level is monitored by averaging 256 samples of V_{MID} that are digitized with the 11b ADC of the BLE module and transmitting the results back to the UBS. Custom alerts can be created on the UBS to notify the user when supply level reaches a pre-specified critical value.

To verify the functionality of the BLE-enabled wireless link in remote programming the ASIC functions from the UBS, representative benchtop tests were performed in which the ASIC was initially configured in its normal operating mode for stimulating on all four channels at a stimulus rate of ~33 Hz and current level of ~40 μA. Additionally, the wired and RF-FSK wireless links of the ASIC were disabled under the normal operating mode. In our first experiment, programming data were compiled on and commanded from the UBS to remotely turn ON/OFF the wired and wireless links of the ASIC via the BLE module.

Figure 13 shows the measured signals in various phases of the system operation that are time-synchronized with the measured instantaneous system current (in mA). Prior to the first programming event, the wired and wireless links of the ASIC were disabled, and the BLE module was configured to advertise its identification information once every second. This can be clearly seen by the three large current peaks of ~4.4 mA occurring once every second. The measured average system current prior to the first programming event was ~172 μA in which the SAMB11 BLE module consumed 13.2 μA during advertising and idle modes, whereas the buck converter and the level shifter consumed 155 μA and 3.8 μA, respectively. For the first programming event (i.e., turn ON the ASIC wired link), the UBS first established a BLE connection and then initiated a programming command for the MCU via the BLE module. Once ASIC programming was performed successfully, an acknowledgment signal was sent by the MCU to the BLE module for relaying back to the UBS upon which the BLE connection was severed. As seen in **Fig. 13**, within the duration of this programming event (~2.68 sec), the system consumed an average of 764 μA, 42.9% of which was due to the BLE module. Ultimately, upon the termination of this programming event, the measured average system current increased from the previous baseline of ~172 μA to a new higher level of ~519 μA, indicating successful engagement of the ASIC's wired link. Next, for the second programming event, the ASIC wired and wireless links were turned OFF and ON, respectively. The same sequence of events repeated shortly after t = 10 sec, which decreased the measured average system current by 133 μA to ~386 μA. A final programming event turned OFF both wired and wireless links of the ASIC, returning the average system current to the baseline level of ~172 μA.

In our second experiment, the BLE-enabled wireless link was used to remotely change the stimulus current level of the ASIC from the UBS. As seen in **Fig. 14**, from the time that the UBS initiated the programming command, it took < 0.8 sec to successfully update the programming status back at the UBS, although it should be noted that the ASIC stimulus current changed (from a maximum level of 94 μA to 46 μA) almost instantaneously once the MCU received and validated the programming data from the UBS. Collectively, these tests established the overall functionality and fast response time of the BLE-enabled wireless link for remote ASIC programming. The system consumed a total of 618.2 μW during its normal operation mode, with the ASIC and the two LDOs consuming 405 μW while the BLE module and the MCU consumed 71.6 μW. The system lifetime for continuous operation in its normal mode was estimated to be > 8 months based on our battery lifetime tests, although this estimate is subject to change based on the rate of use of the wired/wireless links of the ASIC and the level of the output stimulus current. It should also be noted that the BLE transmission range in all aforementioned experiments was ~3.6 meters (i.e., 12 ft).

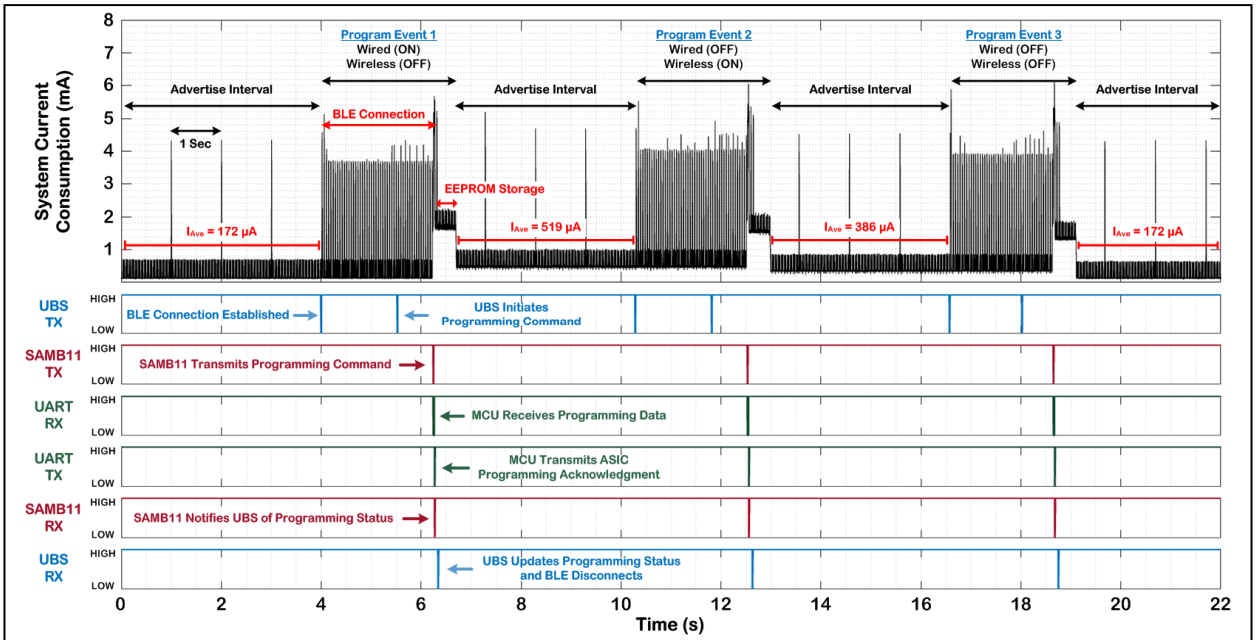

Figure 13: *Measured signals in various phases of system operation during BLE-enabled wireless ASIC programming from user base station, resulting in successful toggling of ASIC operation between the wired and RF-FSK wireless modes, as reflected in the measured instantaneous system current consumption.*

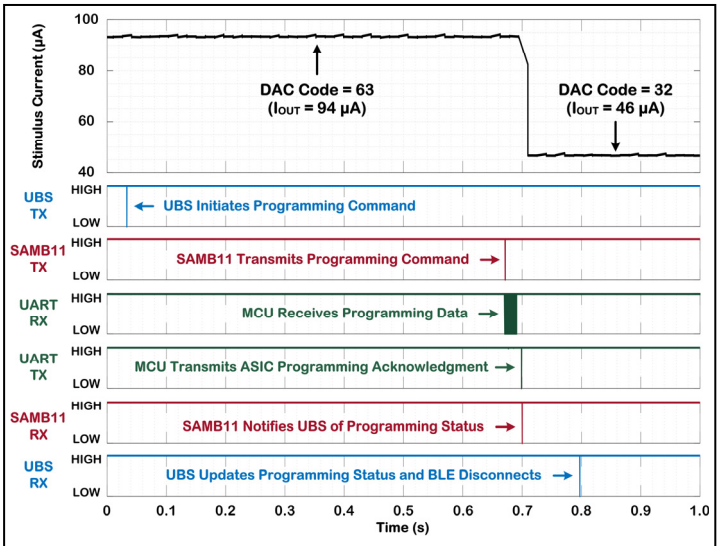

Figure 14: *Measured signals in various phases of system operation during BLE-enabled wireless ASIC programming from user base station, resulting in successful re-programming of the ASIC stimulus current from maximum level of ~94 µA to ~46 µA.*

NHP microdevice development, assembly, & packaging: The NHP microdevice was envisioned to comprise miniaturized backpack and head-mounted units outfitted with custom enclosures. **Figure 15** shows an illustration of the two units along with a UBS equipped with an RF-FSK receiver (@ ~433 MHz) to capture neural recordings from the ASIC in real time. The head-mounted unit (HMU) is placed in a custom, resin, 3D-printed chamber that is affixed to the primate's skull and interfaced with two brain-implanted recording and stimulating microelectrodes. The backpack unit (BPU) is worn on the primate's back, contains power-management circuitry and the BLE module, and is connected to the HMU via a subcutaneously tunneled cable bundle.

The BPU is assembled onto a custom, 4-layer, rigid, printed-circuit board measuring 5.35 cm × 2.90 cm. The fully assembled BPU, weighing 35.5 g including a lithium-ion battery, is then placed inside an off-the-shelf plastic enclosure box (1551H, *Hammond Manufacturing*) measuring 5.91 cm × 3.43 cm × 2.00 cm. Furthermore, the enclosed unit can be easily slipped into a lightweight primate jacket, which can be accessed to replace the device battery or probe various device diagnostic points. The BPU is also coated with a thin, acrylic, conformal coating (419D, *MG Chemicals*) to protect its sensitive circuitry from potential moisture buildup due to elevated humidity and temperature encountered during *in vivo* experimentation.

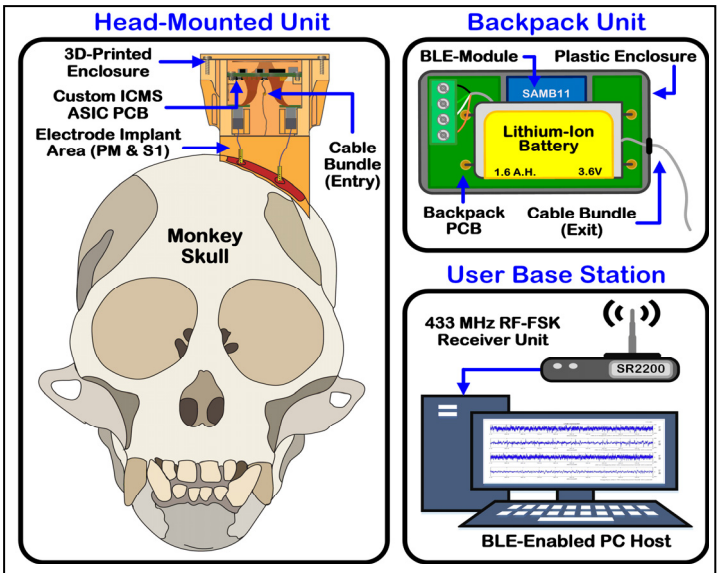

Figure 15: *Illustration of an NHP skull instrumented with a wearable neural microdevice comprised of a head-mounted unit, BLE-enabled backpack unit, and user base station.*

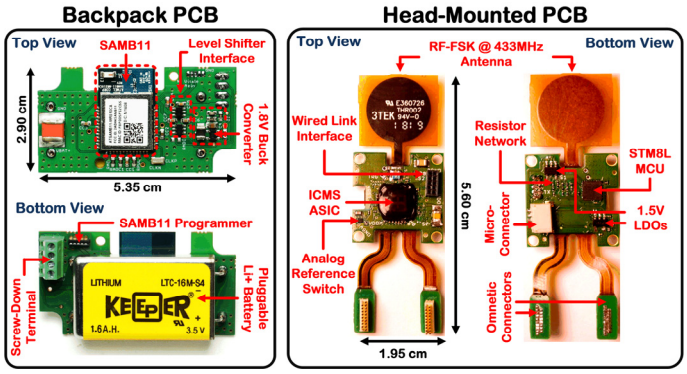

Figure 16: *Photographs of the fabricated and fully assembled backpack and head-mounted printed-circuit boards (PCBs).*

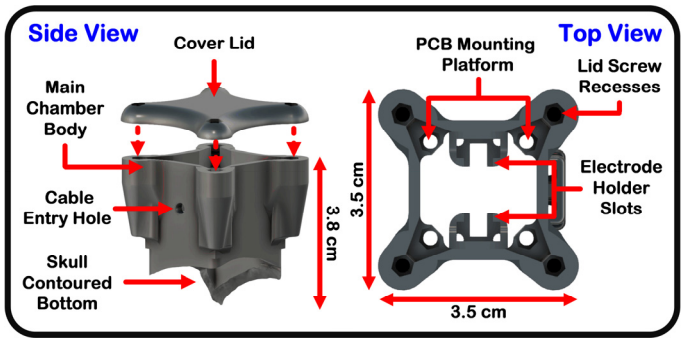

Figure 17: *AutoCAD rendering of the resin, 3D-printed, head-mounted, primate chamber. Hex-shaped recesses allow for the HMU board and a lid to be screwed into place.*

The HMU is assembled onto a custom, 4-layer, rigid-flex, printed-circuit board with the ASIC wirebonded into place and protected with a high-temperature epoxy encapsulant. The board measures 5.57 cm × 1.95 cm × 0.90 cm, including the flexible extrusions at the top and bottom. At the top of the board, a 1.7 cm × 1.5 cm polyimide arm encloses a flexible antenna for RF-FSK transmission. At the bottom, two polyimide arms exit from the main board and terminate into two 9.5 cm × 4.5 cm rigid islands, each populated with a microconnector (A79039-001, *Omentics*) that interfaces directly with a brain-implanted recording or stimulating microelectrode. The HMU weighs 12.5 g, with the chamber accounting for ~87% of the weight. To operate the HMU, a shielded, 4-conductor, PVC-jacketed cable (NMUF4/36-2550SJ, *Cooner Wire*) is subcutaneously tunneled from the BPU's header terminal to provide power, serial communication, and ground signals. The cable is outfitted with a low-profile microconnector, which terminates into a receptacle at the bottom of the HMU board. This allows the HMU to be readily removed in case of microdevice failure without disturbing any other system components such as the BPU or the cable.

Figure 17 depicts an AutoCAD rendering of a custom, resin, 3D-printed chamber measuring 3.5 cm × 3.5 cm × 3.8 cm. This chamber protects the HMU board and creates a sterile barrier between the external environment and the exposed implant area. To minimize pathways for infection around the implant site, the chamber's bottom side is contoured to follow the topography of an adult squirrel monkey's skull. Directly above the skull-contoured region, two slots protrude from the chamber's inner walls to hold the electrode connectors in place. Next, four standoff hex-shaped recesses create a mounting platform for the HMU board. A small opening slightly beneath the platform allows the subcutaneously tunneled cable bundle to enter the chamber and terminate into the HMU board. Finally, a lid is attached to the chamber with a set of screws.

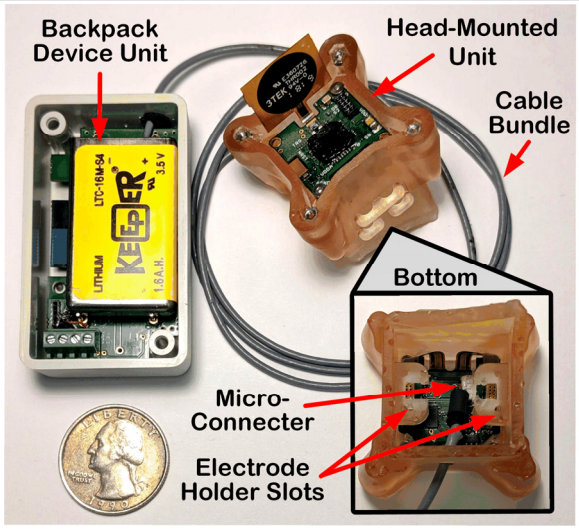

Figure 18: *Photograph of fully assembled backpack and head-mounted units connected by an implantable cable bundle. Lids accompany both units when deployed.*

A silicone sheet is added between the chamber and lid to act as a watertight gasket allowing a complete seal of the chamber once closed.

Before affixing the chamber to the primate's skull, the entire system is assembled into a single monolithic unit as shown in **Fig. 18**. First, the microelectrode shanks are lowered into their respective slot holders. Next, a portion of the cable is threaded through the chamber's entry hole and connected to the HMU board, which is then lowered into the chamber with the flexible arms bent underneath the board to interface with the electrodes' microconnectors. Once the microconnectors are seated, the HMU board is fixed onto the standoff platform with screws. The flexible antenna is then bent over the board, and the lid is screwed into place. The final unit is sterilized with ethylene oxide (EtO) gas and attached to the skull with dental acrylic. Finally, the cable bundle is guided subcutaneously from the HMU toward the BPU located in a primate jacket. The entire microdevice weighs ~48 g.

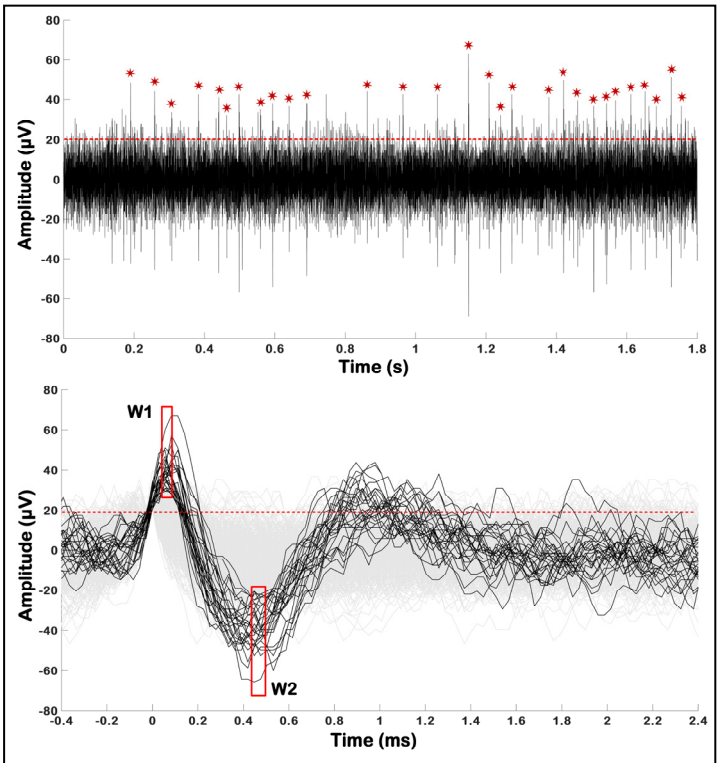

Figure 19: Top – *1.8-sec window of recorded neural activity from saline. Red stars indicate the neural waveforms accepted by the ASIC's spike discriminator.* ***Bottom –*** *Graph of superimposed time-aligned neural waveforms from the recording above. Spike waveforms that satisfy the discrimination criteria are plotted in black, while rejected waveforms are plotted in light gray.*

To verify the overall functionality of the microdevice, *in vitro* experiments were conducted with the system configured as depicted in **Fig. 18**. Acute microelectrode arrays were attached to the HMU board and submerged in saline. In each experiment, digitized neural activity prerecorded from the CFA of freely moving rodents was played into the saline solution, with a silver-chloride wire as the return electrode. In the first phase of experimentation, raw 4-channel recordings were analyzed in LabVIEW via the ASIC's wired link interface. **Figure 19** (top) depicts a 1.8-sec snippet of raw recordings obtained from channel 0. These recordings were then processed offline with a custom script to obtain the parameters for spike discrimination based on thresholding and time-amplitude windowing. These parameters were then wirelessly programmed into the ASIC, and the recording process was repeated. **Figure 19** (bottom) depicts a graph of superimposed time-aligned neural signals detected during the recording. It can be observed that the accepted waveforms (indicated with red stars (top) and in black (bottom)) satisfied all the criteria for thresholding/time-

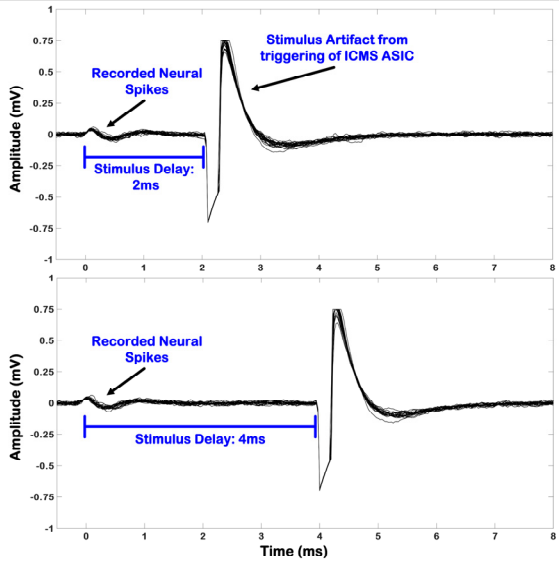

Figure 20: *In vitro demonstration of ADS with spike-stimulus delays of 2 ms and 4 ms. Voltage levels are input-referred.*

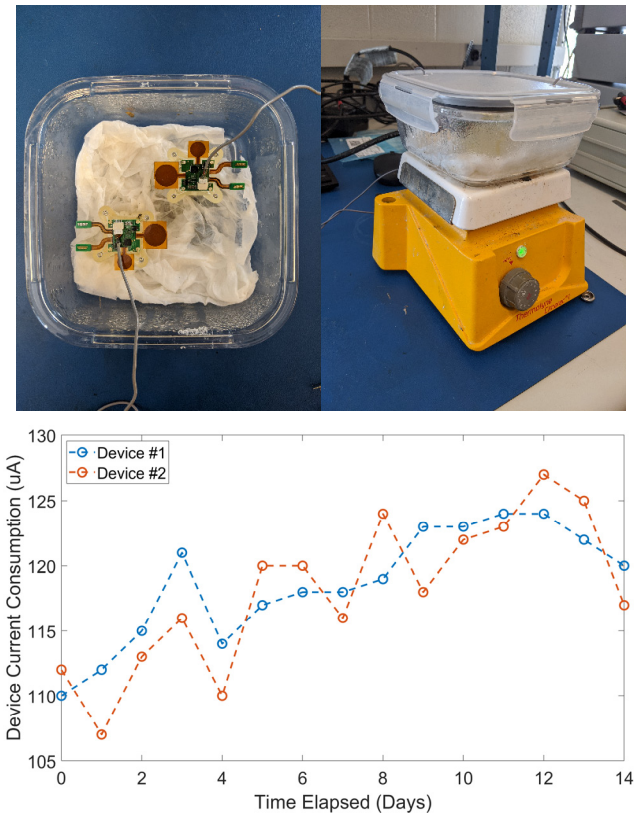

Figure 21: *In vitro setup for encapsulation humidity testing and current consumption of two Parylene–C-coated NHP microdevices over a 2-week period.*

amplitude window discrimination, while other waveforms (in light gray) were rejected for not meeting all of the criteria.

In the second phase of experimentation, the ASIC's stimulating back-end and RF-FSK wireless link were verified. The ASIC was programmed with the spike discrimination parameters obtained in the first phase to trigger stimulation based on discriminated neural spikes on channel 0. Furthermore, for each trigger event, a single monophasic current pulse (40 µA, 192 µs) with passive discharge was delivered through the stimulating electrode to saline. Additionally, the stimulus event was followed by a 3.5-ms blanking period (i.e., neural waveforms occurring after the stimulus event were ignored). **Figure 20** shows graphs of superimposed discriminated neural spike waveforms, obtained via the wireless link, along with their corresponding stimulus artifacts from the single-pulse stimulation with spike-stimulus delays of 2 ms and 4 ms, demonstrating correct functionality of the NHP microdevice for ADS.

HMU hermetic packaging: To protect the sensitive circuitry of the HMU from potential moisture buildup and to limit liquid and vapor water ingress due to elevated humidity and temperature encountered during *in vivo* experimentation, the HMU board was encapsulated by a 5-µm layer of Parylene–C applied via chemical vapor deposition (CVD, *SMART Microsystems*). Prior to deposition, the board was cleaned in a 50°C ultrasonic bath consisting of 10% flux solvent (*MG Chemicals*) and 90% de-ionized water by volume, which was done to ensure the removal of contaminants that may have interfered with layer adhesion or facilitated corrosion due to metal-ion reactions. The effectiveness of the Parylene–C encapsulant was verified *in vitro* on partially populated test boards, which were absent of the ASIC and the two Omnetics microconnectors. Levels of moisture ingress were observed by monitoring microdevice current consumption, as well as by shorting the primary stimulation sites to the 1.8-V rail in order to monitor internal resistance changes through the microdevice's site impedance-monitoring function. Two microdevices were prepared, cleaned, and coated before being placed into a covered glass container lined with damp towels and placed on a hotplate in order to generate an elevated temperature

and humidity environment (**Fig. 21**). Each board was rested upon one of the resin 3D-printed chambers to prevent direct contact with the heat or moisture source, while still allowing ample vapor circulation to both sides of the board. Over a 2-week monitoring period, current consumption of both microdevices demonstrated an average fluctuation of less than ±5% (**Fig. 21**), with no observed deviation of stimulation site voltages from their 1.8-V baseline value.

Major Task 6: Conduct preclinical efficacy study in ambulatory non-human primates

Subtask 1: Complete institutional IACUC and ACURO review process: This milestone (i.e., obtain approval for animal protocol) was achieved on 08/23/2017, covering the animal care and use for all the specific aims.

Subtask 2: Conduct ambulatory experiments in non-human primates (Aim 3): *Rationale:* Aim 3 was designed as a controlled study of the effects of ADS on motor recovery after a CCI injury in NHPs. Translation of the rodent results to a primate model is critical for further justification of device development for humans. As the NHP microdevice was still under development at the time of Aim 3 initiation, we decided to optimize our CCI techniques and conduct a study to examine motor deficits and recovery in three squirrel monkeys in the control group. This was a reasonable approach, because long-term behavioral performance after a CCI injury in NHPs had not been conducted before.

Study design: The main endpoint of this Aim consisted of recovery profiles on two behavioral tasks designed to assess hand dexterity and grip performance.

1. *Hand dexterity*. Hand dexterity was assessed using a modified Klüver board. This task is a modified version of one used in other studies to examine grasping of small food items after cortical injury (Nudo, et al., 1996; **Fig. 22A**).

2. *Grip performance.* The grip apparatus consisted of an aluminum cylinder connected to a universal joint allowing the cylinder to rotate in multiple directions as described in a previous publication (Bury, et al., 2009; **Fig. 22B**). To obtain a food reward, the monkey had to squeeze the handle activating the force transducer, applying a specified range of force and time. Food pellets were delivered to a food bin placed within the monkey's cage once the handle was released. The monkey could make as many grips as possible during a 30-min session on a "Difficult" task and during a 5-min session on an "Easy" task (see **Fig. 22** caption). Monkeys were trained on the behavioral task until stable baseline performance was achieved. After the CCI injury, monkeys were tested once per week for 13 weeks.

Controlled cortical impact (CCI) procedures: Somatosensory and motor mapping techniques were used to define the regions of interest in primary motor cortex, premotor cortex, and somatosensory cortex as described in other publications (Dancause, et al., 2005). A commercial electromagnetic impact device (Impact One, Leica Biosystems, Buffalo Grove, IL) was used to deliver a TBI to the distal hand representation of M1. The impact parameters were based on our previous studies using CCI procedures in rats (Nishibe, et al., 2010). The impactor tip was a stainless-steel rod with a 5-mm diameter (slightly beveled to remove sharp edges around the perimeter). The impact was delivered over the M1 hand area with a depth of 3 mm from the cortical surface at 4.5 m/s with a dwell time of 200 ms.

Neurophysiological verification of injury: At the end of the 13-week post-injury period, under anesthesia in a terminal procedure, neural recordings were collected to assess viability of the injured area.

Results: CCI lesions were made over the M1 hand area in three monkeys (**Fig. 23A**). Neurophysiological verification was performed in two of the three monkeys. One additional animal died during the anesthetic protocol. In each of the three monkeys with CCI injuries, the cortical territory at the site of impact appeared shrunken three months after the CCI. Intracortical microstimulation (ICMS) techniques confirmed that no movements could be evoked within the distal forelimb representation in M1 (**Fig. 23B**). Neural recordings were taken within and adjacent to the impact area to compare spiking activity between motor cortical areas. Neural activity within the remaining tissue within the impact zone showed less spontaneous spiking activity than tissue outside the area of impact (**Fig. 23C**).

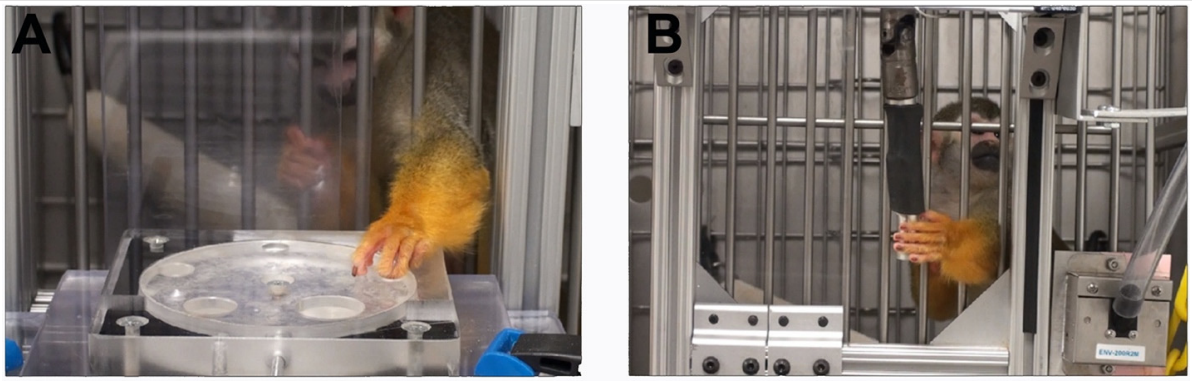

Figure 22: *Motor skill assessment apparatus.* ***A.*** *Modified Klüver board apparatus. This task is used to train and assess hand dexterity during a reach and retrieval task. Monkeys were required to retrieve a single 45-mg food pellet (3.56-mm diameter) delivered singularly to five food wells. Each food well was 5 mm deep ranged in diameter from 25 mm to 9.5 mm.* ***B.*** *Hand grip apparatus. This task was used to assess ability of monkeys to apply and sustain a predetermined grip force within a range of either 100–300 g of force for 10 sec ("Difficult" task) or 20–500 g of force for 0.5 sec ("easy" task). A food pellet was delivered automatically for each execution of the selected task.*

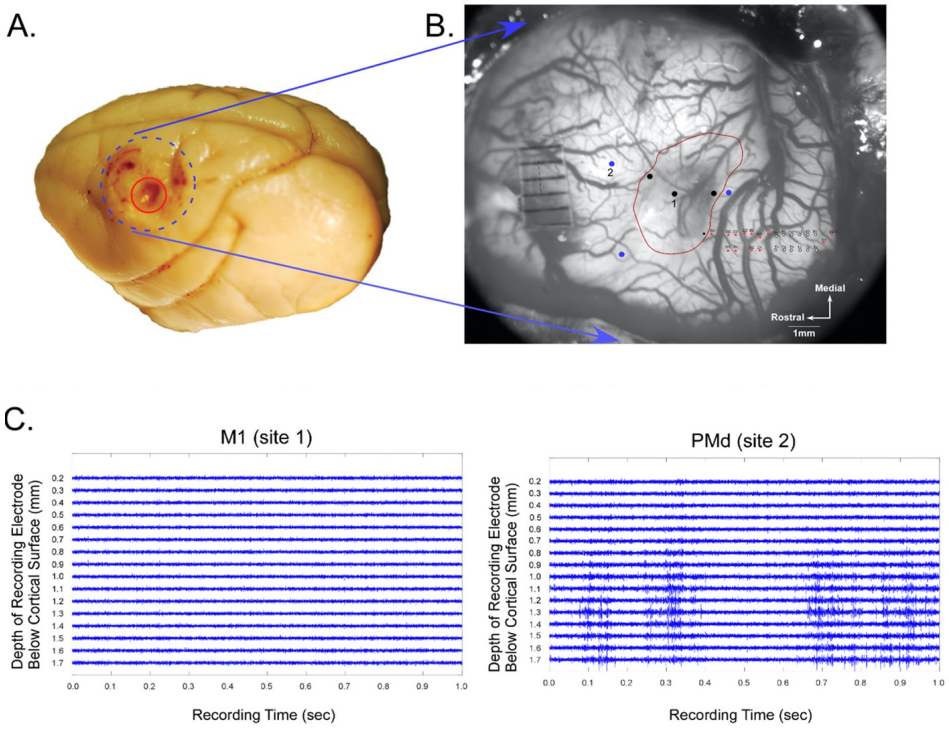

Figure 23: *CCI injury three months post-injury.* ***A.*** *Post-mortem photograph of dorsolateral surface of cortex in squirrel monkey A401. CCI injury can readily be seen within the red circle. The blue dashed circle indicates the position of the craniectomy made during the initial procedure to access cerebral cortex for identifying M1 and adjacent motor and somatosensory areas.* ***B.*** *Intraoperative photograph of cortical surface with superimposed neurophysiological data. Large red outline shows distortion of lesion area 3 months after CCI. ICMS techniques verified that movements could be evoked from premotor areas (large blue filled circles), but not from the injured area in M1 (large black filled circles). Cutaneous responses were also obtained in primary somatosensory cortex (small red and white dots in lower right).* ***C.*** *Neural spike recordings from inside impact area labeled "1" and outside impact area labeled "2". Cortical activity during a 1-sec sample is shown for 16 channels acquired from depths of 200 to 1,700 µm (left side of each figure). Very little spontaneous spiking activity was observed within the impact area (Site 1) compared to an adjacent non-impacted area (Site 2), verifying that the CCI injury damaged the M1 hand area but the premotor area was still intact.*

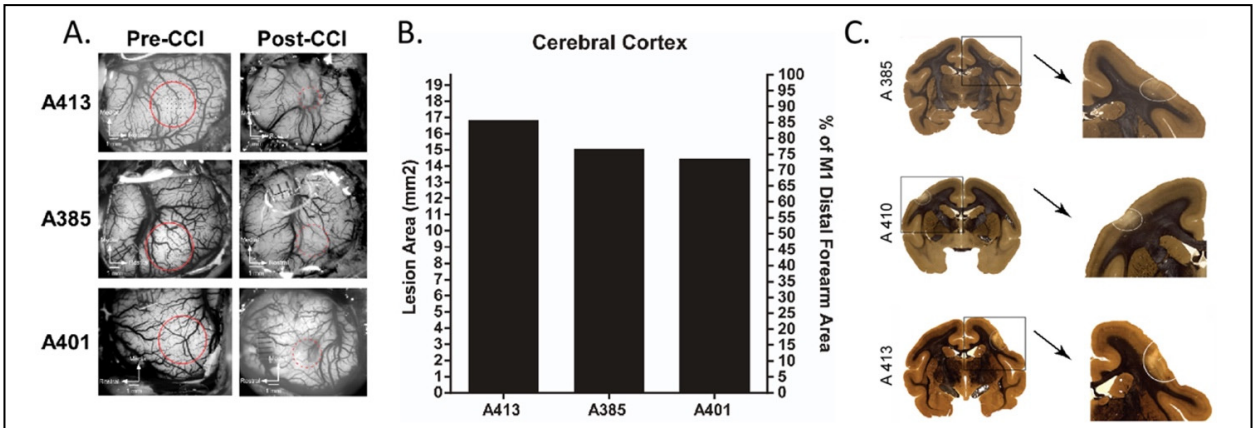

Figure 24: A. *Surface area of cerebral cortex. Solid red outline identifies target for CCI before impact in Pre-CCI column whereas a dashed red circle identifies the corresponding cortical surface (based on vascular patterns) 3 months after impact in Post-CCI column.* ***B.*** *Cortical area under impact was reduced by 85.6% (16.8 mm^2) for monkey A413, 76.7% (15.1 mm^2) for monkey A385, and 73.6% (14.5 mm^2) for monkey A401.* ***C.*** *Coronal Sections (Weil stain). First column shows photos (2.5×) of the coronal section for all three monkeys. Second column is a larger view of the location of impact for each monkey. The Weil stained sections were used to estimate area of the corona radiata underlying the area of cortical infarct.*

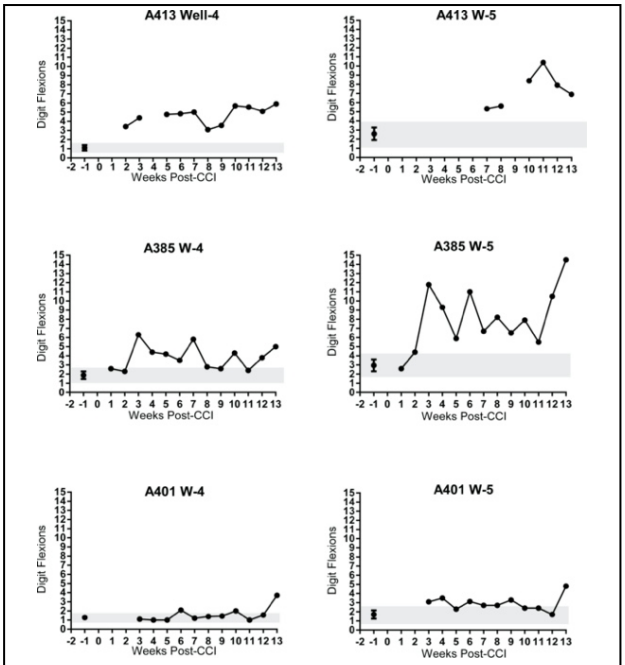

Figure 25: *Hand dexterity for retrieving food pellets from wells 4 (left: 11.5-mm dia.) and 5 (right: 9.5-mm dia.) on Klüver Board Task. Skill levels were determined relative to each monkey's average pre-injury baseline distribution of scores over five sessions collected over a two-week period prior to CCI injury. Baseline performance (95% confidence interval, CI) is indicated in the grey shaded area. Scores above the shaded area indicate significantly impaired performance.*

Comparison of pre-CCI and three-month post-CCI injury demonstrated a reduction in impacted cortical surface area in each monkey (**Fig. 24**). There was a reduction in impacted DFL/M1 cortex in each monkey exceeding 70% of the impacted area: A401 loss 73.6%, A385 loss 76.7%, and A413 loss 85.6%. Estimated volume of white matter within the corona radiata beneath DFL/M1 indicated a loss of fibers in each monkey. The volume of corona radiata underlying the injured cortex was reduced by 5.29% for A401, 4.10% for A385, and 11.66% for A413.

Hand dexterity after CCI injury: The ability to successfully reach and retrieve pellets from each of the five food wells varied among the three monkeys after the CCI injury (**Fig. 25**). Two of the three monkeys (A413 and A401) could not successfully retrieve a food pellet from any of the wells initially after the CCI. A413 was able to perform the task by the second week after the injury and A401 was able to perform the task by the third week after the injury. Difficulty in grasping and retrieving food pellets from the food wells persisted as measured by the number of finger flexions required to extract and retrieve a food pellet. Impairment in extracting food pellets lasted through the entire 13 weeks of post-CCI assessment. Even though extracting the food pellets from the larger food wells (wells 1 to 3) were affected by the impact, all monkeys could extract food pellets with one or two flexions by third

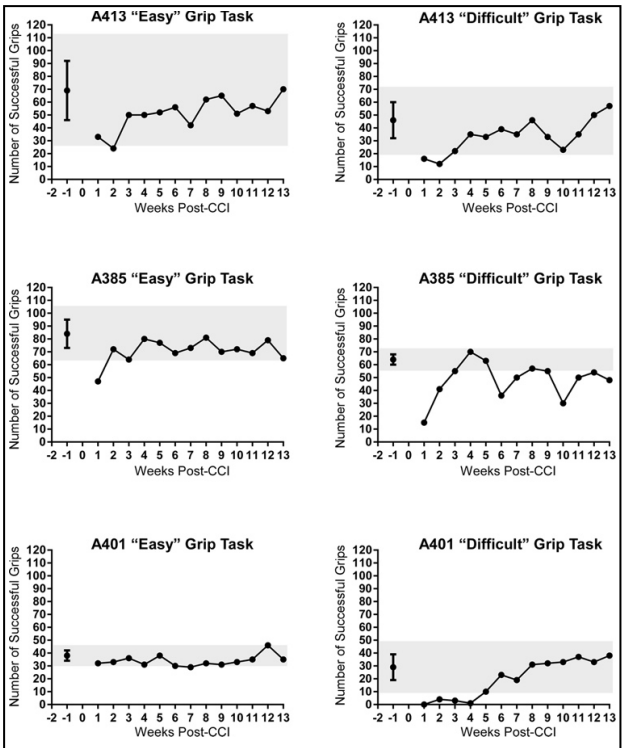

Figure 26: *Performance on hand grip task pre- and post-CCI. Numbers of successful grips on a given weekly session (1 to 13) were converted to z-scores standardized to the mean and standard deviation of the individual monkey's baseline distribution. The 95% CI for each monkey is designated by the grey shaded area. Scores falling below the shaded area (z = 2.0) indicated significantly worse performance compared to baseline. All monkeys were impaired on the "Difficult Task" but recovered to within baseline values between 3 and 6 weeks.*

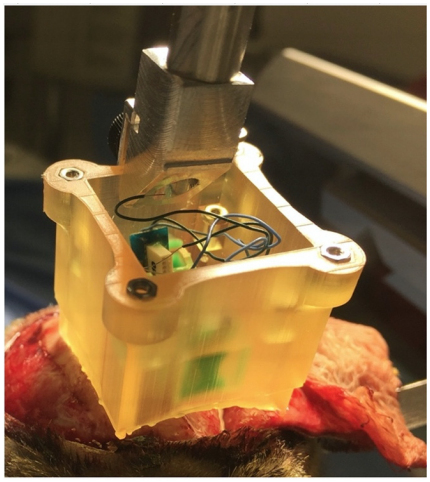

Figure 27: *Intraoperative photograph of custom chamber containing microdevice mounted on the head of a monkey.*

week of recovery. Impaired motor skills were more pronounced for extracting food pellets from the smallest wells (wells 4 and 5).

Grip performance – Easy task: During the first week after CCI, monkeys A413 and A385 had difficulty maintaining a grip between 25–500 g for 0.5 sec (**Fig. 26**). This difficulty persisted for A413 for the second week. A401 was able to perform the easy task within his baseline range. Within the first month after injury, A413 and A385 recovered to near baseline performance level on the "Easy" task. A401 never showed any significant deviation from baseline on the "Easy" task except in week 7 post-CCI assessment.

Grip performance – Difficult task: Prior to the CCI, all three monkeys were able to sustain the hand grip force between 100 and 300 g for 3 sec (**Fig. 26**). During the first week after CCI, each of the monkeys had difficulty reaching the 100-g threshold and maintaining grip at the required force and duration. Grip performance of A413 and A401 recovered to within the baseline range by 4 and 6 weeks, respectively. In A385, performance was more variable, with normal performance met on only weeks 5 and 6.

Discussion and conclusions: We have shown that we can create reliable lesions in motor cortex using the CCI technique that has previously been used primarily in rodent models. To our knowledge, this is the first study examining long-term behavioral recovery after CCI lesions in NHPs. Using the impact parameters used in this study of untreated control animals, we were able to demonstrate chronic mild-to-moderate impairments in hand dexterity. However, grip performance recovered within a few weeks in 2 of the 3 monkeys. These results suggest that these impact parameters will be useful for comparing the effects of ADS therapy to untreated control animals. However, more severe chronic impairments would be desirable for discriminating the effects of treatment. Thus, a larger impactor tip, greater velocity, and greater impact depth should be considered in future studies.

Current status: This study of the effects of CCI injury in an NHP model is complete and the manuscript is now being finalized. It will be submitted for publication by the end of March 2021.

Successful implantation of microelectrodes, microdevice, and chamber attachment: In a terminal procedure in a squirrel monkey, the sterilized microelectrodes/microdevice/chamber

unit was attached to a stereotaxic arm and positioned over the cranial opening (**Fig. 27**). Using forceps, each microelectrode was positioned directly over either the ventral premotor cortex (for recording) or S1 (for stimulating) based on the vascular pattern and the previously derived motor and sensory maps. Once the microelectrodes were seated, the entire opening was flooded with Kwik-Cast silicone polymer to fix them in place relative to the surface of the brain and to completely seal the cranial opening. Once the polymer became fixed, the chamber was then lowered onto the surface of the skull. A universal joint on the stereotaxic arm allowed the chamber position to more closely approximate the curvature of the remaining skull. The chamber was then successfully affixed to the skull using bone cement to form a seal between the outside and inside of the chamber. The signal and power wires were threaded out an opening in the chamber, and then this opening was also sealed with the silicone polymer. Once the chamber was fixed, the cable bundle containing the power and signal wires was subcutaneously tunneled under the scalp, down the neck, and exited mid-back to a position where it could be connected to the battery supply and programming board of the BPU located in a mesh primate jacket. The skin around the chamber was sutured and post-operative analgesics were administered. Prior to post-operative recovery, acute testing of the microdevice was performed to verify its functionality and communications to external hardware. Collectively, these results demonstrate that the chamber design and implantation procedures are feasible for completing the NHP studies.

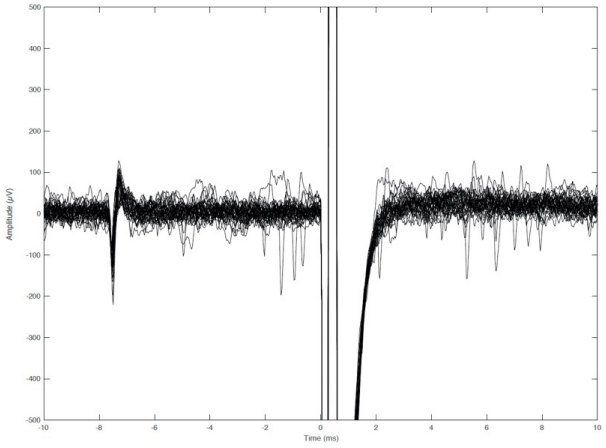

Figure 28: *Recordings of neural spikes detected in premotor cortex in an anesthetized squirrel monkey. Several traces are superimposed. Detected neural spikes are shown at ~ -7.5 ms. Stimulus artifact from stimulation pulse in S1 is shown beginning at ~ 0 ms.*

Successful implementation of ADS in a squirrel monkey: As the development of the microdevice was still undergoing refinement to address some of the unforeseen challenges of *in vivo* deployment in an ambulatory NHP model, we tested our ability to implement ADS in a terminal procedure in one squirrel monkey under anesthesia. Using a time-amplitude window discriminator programmed into a field-programmable gate array (FPGA) that was functionally equivalent to the microdevice, we were able to perform a de-risking study to ensure that there were no abnormal responses in the PMv-Area 2 loop. We were able to reliably set parameters for spike discrimination, reliably detect extracellular neural spikes, and use spike discharges to trigger stimulation in a distant area with pre-determined delays, as we previously did in rodents (**Fig. 28**).

Overall conclusions: We successfully completed the rodent aims and demonstrated that ADS was effective even when treatment was delayed up to 3 weeks post-injury. With the one-week post-injury initiation, 4 weeks of treatment resulted in recovery of motor performance that persisted for 8 weeks, the total duration of the follow-up period. Moreover, we were able to develop a fully assembled and packaged NHP microdevice that was small enough to be housed within a chronic, skull-affixed, primate chamber. Over a 2-week monitoring period, the NHP microdevice remained fully functional in a simulated *in vivo* environment with elevated humidity and temperature. Finally, we were able to demonstrate the first NHP model of CCI injury designed for long-term behavioral assessment. We established procedures for implantation of the NHP microdevice within a chronic chamber and for microelectrodes implantation in target cortical locations. We also demonstrated that we could perform spike-triggered stimulation reliably in a squirrel monkey. We are now in an excellent position to test the ability of ADS to enhance behavioral recovery after such injuries.

Bibliography

Azin M, Guggenmos DJ, Barbay S, Nudo RJ, Mohseni P. A battery-powered activity-dependent intracortical microstimulation IC for brain-machine-brain interface. Solid-State Circuits, IEEE Journal of. 2011a; 46(4):731-45. doi: 10.1109/JSSC.2011.2108770.

Azin M, Guggenmos DJ, Barbay S, Nudo RJ, Mohseni P. A miniaturized system for spike-triggered intracortical microstimulation in an ambulatory rat. Biomedical Engineering, IEEE Transactions on. 2011b; 58(9):2589-97. doi: 10.1109/TBME.2011.2159603.

Bury SD, Plautz EJ, Liu W, Quaney BM, Luchies CW, Maletsky RA, Nudo RJ. A novel device to measure power grip forces in squirrel monkeys. J Neurosci Methods. 2009 May 15; 179(2):264-70. doi: 10.1016/j.jneumeth.2009.02.003. Epub 2009 Feb 13. PMID: 19428536; PMCID: PMC2700290.

Dancause N, Barbay S, Frost SB, Plautz EJ, Chen D, Zoubina EV, Stowe AM, Nudo RJ. Extensive cortical rewiring after brain injury. J Neurosci. 2005 Nov 2; 25(44):10167-79. doi: 10.1523/JNEUROSCI.3256-05.2005. PMID: 16267224; PMCID: PMC6725801.

Guggenmos DJ, Azin M, Barbay S, Mahnken JD, Dunham C, Mohseni P, Nudo RJ. Restoration of function after brain damage using a neural prosthesis. Proc Natl Acad Sci USA. 2013 Dec 24; 110(52):21177-82. doi: 10.1073/pnas.1316885110. Epub 2013 Dec 9. PMID: 24324155; PMCID: PMC3876197.

Hudson HM, Guggenmos DJ, Vitale N, Azin M, Mohseni P, Nudo RJ (2019) Optimal post-injury time window to apply activity-dependent stimulation to drive functional recovery after traumatic brain injury in the rat. Program No. 584.01. 2019 Neuroscience Meeting Planner. Chicago, IL: Society for Neuroscience, 2019. Online.

Nishibe M, Barbay S, Guggenmos D, Nudo RJ. Reorganization of motor cortex after controlled cortical impact in rats and implications for functional recovery. J Neurotrauma. 2010 Dec; 27(12):2221-32. doi: 10.1089/neu.2010.1456. Epub 2010 Nov 22. PMID: 20873958; PMCID: PMC2996815.

Nudo RJ, Wise BM, SiFuentes F, Milliken GW. Neural substrates for the effects of rehabilitative training on motor recovery after ischemic infarct. Science. 1996 Jun 21; 272(5269):1791-4. doi: 10.1126/science.272.5269.1791. PMID: 8650578.

What opportunities for training and professional development has the project provided?

Five electrical engineering graduate students at CWRU were trained on a wide range of salient topics, including the development of a wireless link based on a Bluetooth Low Energy (BLE) module for neural interface microdevices, neural signal processing, design of implantable microsystems for biopotential recording, hermetic assembly/packaging of implantable microsystems, and methods of powering/communicating with them. The students also had many opportunities for professional development by attending various technical and scientific conferences of the IEEE in 2017–2020.
One research analyst and one postdoctoral fellow at KUMC were trained on creating data management systems and developing data analytic tools, as well as on developing IACUC protocols for regulatory approvals, experimental testing of neural interface microdevices, and performing behavioral training, surgical procedures, and post-operative behavioral assessment and analysis.

How were the results disseminated to communities of interest?

Results were presented at the IEEE Biomedical Circuits and Systems (BioCAS) conference that took place in Cleveland, OH in October 2018. PI Mohseni served as the General co-Chair of the conference. Results were disseminated in the form of a poster presentation and live demonstration of a functional prototype microdevice developed for non-human primate studies.

N. H. Vitale, M. Azin, and P. Mohseni, "A Bluetooth Low Energy (BLE)-enabled wireless link for bidirectional communications with a neural microsystem," in *Proc. IEEE Biomed. Circ. Syst. Conf. (BioCAS)*, pp. 371-374, Cleveland, OH, October 17-19, 2018 **(Selected for presentation in *Live Demonstrations* session)**.

Furthermore, neurobiological results were presented at the 2019 Society for Neuroscience Symposium in the form of a published abstract and a presented poster.

Hudson HM, Guggenmos DJ, Vitale N, Azin M, Mohseni P, Nudo RJ (2019) Optimal post-injury time window to apply activity-dependent stimulation to drive functional recovery after traumatic brain injury in the rat. Program No. 584.01. 2019 Neuroscience Meeting Planner. Chicago, IL: Society for Neuroscience, 2019. Online.

What do you plan to do during the next reporting period to accomplish the goals?

Nothing to report.

4. IMPACT:

What was the impact on the development of the principal discipline(s) of the project?

Our work in this project yielded one of the smallest, most lightweight microdevices for activity-dependent stimulation (ADS) in a rat model of traumatic brain injury (TBI). Results from our experiments in rats with TBI undergoing ADS treatment demonstrated rapid and significant recovery of motor performance as expected. More importantly, our results revealed that ADS treatment could be delayed up to 3 weeks after injury, while still improving the motor performance. Moreover, our results showed no drop in motor performance eight weeks after ADS treatment ended in rats that started to receive the therapy 1 week after injury. Optimal design strategies for a fully enclosed, skull-mounted, non-human primate (NHP) microdevice were also devised. Two generations of the NHP microdevices were developed, which were fully functional electrically at the benchtop level, along with techniques for hermetic assembly/packaging of the devices to ensure their long-term functionality during neurobiological experiments *in vivo*. Furthermore, our work in this project yielded a unique controlled cortical impact (CCI) model of TBI in an NHP, resulting in persistent impairments in motor function evident in volitional use of the hand. This is essential to extend current rodent models to the complex neural architecture of the primate brain. Moving forward, this model can be used to investigate novel therapeutic interventions to improve or restore impaired motor function after trauma.

What was the impact on other disciplines?

Nothing to report.

What was the impact on technology transfer?

Profs. Mohseni and Nudo had previously established a start-up company that in 2017 changed its name from Neuralink Technologies LLC to Neurobond Technologies LLC. The name change was made after trademark rights to the name Neuralink were acquired by Mr. Elon Musk for his newly formed company, Neuralink Corp.

What was the impact on society beyond science and technology?

Nothing to report.

5. CHANGES/PROBLEMS:

Changes in approach and reasons for change

Nothing to report.

Actual or anticipated problems or delays and actions or plans to resolve them

.

The CWRU team experienced a delay in submitting their new activity-dependent stimulation (ADS) application-specific integrated circuit (ASIC) design to The MOSIS Services for fabrication. Nonetheless, the design was successfully submitted for fabrication in April 2017 and received in July 2017 (i.e., in Y1Q4). This was not a major concern, because the KUMC team had not yet obtained full ACURO approval to start the preclinical efficacy studies. The KUMC team experienced an administrative delay in the approval of the ACURO protocol (Major Task 2: Subtask 1), which subsequently delayed the start of Major Task 2: Subtask 2. This was not a major concern either, because the ACURO approval would cover Subtask 1 of Major Tasks 2, 4, and 6 simultaneously, reducing administrative delays further down the road. ACURO approval was received in August 2017.

There were some unforeseen delays in constructing the rodent microdevices, including manufacturer-caused delay in fabricating the substrates and supplier-caused delay in providing one type of Omnetics connector that is used with each rodent microdevice for temporary monitoring/programming. These delays were typically about 2-4 weeks and hence not too significant. In addition, the microelectrode array supplier changed the wiring configuration of their electrodes, necessitating an alteration in the microdevice connections that was quickly implemented with success to construct additional microdevices.

We had an unforeseen number of rodent microdevices fail mechanically during the experimentation phase. Because of the limited supply of microdevices at the time, we reduced the number of concurrent animals being run to ensure that microdevices could be replaced, if they failed. There were many discussions about modes of mechanical failure, and a resolution to make more microdevices and to slightly alter the location of the stainless-steel rod mounting on the implant was deemed to effectively address these problems.

Unexpected noise and artifactual signals were also observed in the recorded neural signals during wired operation of a few rodent microdevices, which adversely affected our ability to discriminate spiking activity. Those microdevices and the peripheral equipment were subsequently returned to CWRU to pinpoint the source of the noise/artifacts and determine a solution going forward. The KUMC team suspended all new behavioral testing and microdevice implantations until a solution was found. After 3 weeks of electronic debugging by the CWRU team, the source of these problems was identified and remedial solutions (i.e., additional noise-filtering capacitors) were implemented into the affected microdevices as well as newly assembled batches of microdevices that were subsequently delivered to KUMC to resume the neurobiological experimentations. Our collective efforts ultimately allowed us to complete Major Tasks 1, 2, 3, and 4.

Several unforeseen challenges prevented successful operation of the non-human primate (NHP) microdevice in two rounds of neurobiological experiments at KUMC in Y3Q2 and Y3Q4. First, the subcutaneous cable connecting together the backpack and head-mounted portions of the microdevice was soldered at one end to the head-mounted microdevice inside the 3D-printed, skull-affixed chamber. The epoxy that was used to protect the solder joint expanded in volume over time and displaced a critical component on the rigid-flex substrate that ultimately resulted in premature battery drainage. Second, excessive amount of moisture accumulated inside the skull-affixed chamber that in turn shorted out the electrical components of the rigid-flex substrate, causing microdevice operation failure after several hours of implantation. Third, potential grounding issues in the NHP microdevice deployment caused the output signals to have a higher level of noise than expected.

To mitigate these issues, our efforts focused on modifying the design and construct of the head-mounted portion of the NHP microdevice so that the subcutaneous cable could be connected via a microconnector, obviating a need for soldering and subsequent use of epoxy. We also focused on identifying medical-grade epoxy materials for encapsulation of the entire rigid-flex substrate to protect it against moisture accumulation inside the plastic chamber. This effort in turn necessitated establishing an experimental setup in the CWRU laboratory, for the first time, for accelerated testing of the longevity of various epoxy materials as a function of changes in temperature and moisture content, as well as investigating techniques for effective application of epoxy materials to the rigid-flex substrate.

With regard to the grounding issues, the usual practice was to connect the grounds found on the unused recording and stimulation electrode sites to both the analog ground on the microdevice and the animal body ground obtained by means of an implanted skull screw. There was concern that the multitude of spatially separated grounds may have formed ground loops and alternative current-return pathways that may have distorted the small neural signals. While experimental work on this front was somewhat limited by the ongoing COVID-19 pandemic, the most probable causes of these grounding issues were ascertained nonetheless. This was primarily accomplished through the construction and cooperative analysis of diagrams pertaining to system grounds, current-return pathways, and the surrounding recording environment. Our collective efforts ultimately allowed us to complete Major Task 5, but the ongoing COVID-19 pandemic hampered our efforts toward full completion of Major Task 6.

Specifically, laboratory operations were shut down in April 2020, and visitors were not allowed on campus at KUMC. Thus, planned joint experiments could not be completed anymore. All animal experimentation was temporarily halted as well. This period of reduced experimental activity was used to finalize histological analyses of CCI injuries in Aims 1–3 and to develop manuscripts for publication.

Changes that had a significant impact on expenditures

Since ACURO approval was received in August 2017, which was almost one year after the start date of the award performance period, we required additional time to perform the proposed specific aims with no additional funds being requested. Hence, we successfully obtained approval for a no-cost extension of the performance period until August 31, 2020.

Significant changes in use or care of human subjects, vertebrate animals, biohazards, and/or select agents

Significant changes in use or care of human subjects

Not applicable.

Significant changes in use or care of vertebrate animals

Nothing to report.

Significant changes in use of biohazards and/or select agents

Not applicable.

6. PRODUCTS:

- **Publications, conference papers, and presentations**

  Journal publications.

Nothing to report at this time. Two manuscripts describing results and findings from our rodent experiments as well as results and findings from developing a TBI model in non-human primates with lasting behavioral deficits are currently in the final stage of preparation for submission. Both efforts are being led by the KUMC team.

Books or other non-periodical, one-time publications.

Nicholas H. Vitale
M.S. Thesis Defense: August 7, 2019
Graduation Date: January 2020

ependent

Intracortical Microstimulation in Non-Human Primates
Current Position: Doctoral Student, Dept of Electrical Engineering, Stanford University

Other publications, conference papers, and presentations.

N. H. Vitale, M. Azin, and P. Mohseni, "A Bluetooth Low Energy (BLE)-enabled wireless link for bidirectional communications with a neural microsystem," in *Proc. IEEE Biomed. Circ. Syst. Conf. (BioCAS)*, pp. 371-374, Cleveland, OH, October 17-19, 2018 **(Selected for presentation in *Live Demonstrations* session)**.

A second paper describing the design, development, *in vitro* testing, and assembly/packaging of the BLE-enabled non-human primate microdevice will be submitted in May to the 2021 IEEE BioCAS conference. This effort is being led by the CWRU team.

Hudson HM, Guggenmos DJ, Vitale N, Azin M, Mohseni P, Nudo RJ (2019) Optimal post-injury time window to apply activity-dependent stimulation to drive functional recovery after traumatic brain injury in the rat. Program No. 584.01. 2019 Neuroscience Meeting Planner. Chicago, IL: Society for Neuroscience, 2019. Online.

- **Website(s) or other Internet site(s)**

Nothing to report.

- **Technologies or techniques**

Nothing to report.

- **Inventions, patent applications, and/or licenses**

Nothing to report.

- **Other Products**

Nothing to report.

7. PARTICIPANTS & OTHER COLLABORATING ORGANIZATIONS

What individuals have worked on the project?

Name: Pedram Mohseni
Project Role: PD/PI
Researcher Identifier (e.g. ORCID ID): 0000-0002-2849-4677
Nearest person month worked: 7.2
Contribution to Project: Dr. Mohseni oversaw the project progress related to the development of microdevices at CWRU, and maintained communications with the collaborating team at KUMC.

Name: Randolph Nudo
Project Role: Subaward PI
Researcher Identifier (e.g. ORCID ID): 0000-0002-4674-0907
Nearest person month worked: 3.4
Contribution to Project: Dr. Nudo oversaw the project progress related to the neurobiological studies at KUMC, and maintained communications with the collaborating team at CWRU.

Name: Nicholas Vitale
Project Role: Graduate Student at CWRU
Researcher Identifier (e.g. ORCID ID): -
Nearest person month worked: 36
Contribution to Project: Mr. Vitale has performed work in the area of bidirectional wireless links for the microdevices based on a Bluetooth low energy (BLE) module.

Name: Meysam Azin
Project Role: Independent Contractor for CWRU
Researcher Identifier (e.g. ORCID ID): -
Nearest person month worked: 16
Contribution to Project: Dr. Azin has performed work in the area of algorithms and coding as well as verification of experimental setup reliability and stability.

Name: Chris Delianides
Project Role: Graduate Student at CWRU
Researcher Identifier (e.g. ORCID ID): -
Nearest person month worked -
Contribution to Project: Mr. Delianides has performed work in the area of hermetic packaging of the non-human primate microdevice using a variety of encapsulation materials and techniques.

Name: Reza Erfani
Project Role: Graduate Student at CWRU
Researcher Identifier (e.g. ORCID ID): -
Nearest person month worked: -

Contribution to Project: Mr. Erfani has performed work in the area of wireless powering of biomedical implants.

Name: Fatemeh Marefat
Project Role: Graduate Student at CWRU
Researcher Identifier (e.g. ORCID ID): -
Nearest person month worked: -
Contribution to Project: Ms. Marefat has performed work in the area of integrated circuit development for high-fidelity biopotential recording.

Name: Hossein Zamani
Project Role: Graduate Student at CWRU
Researcher Identifier (e.g. ORCID ID): -
Nearest person month worked: -
Contribution to Project: Mr. Zamani has performed work in the area of neural signal processing for online data compression.

Name: Michael Suster
Project Role: Senior Research Associate at CWRU
Researcher Identifier (e.g. ORCID ID): -
Nearest person month worked -
Contribution to Project: Dr. Suster assisted PD/PI Mohseni in overseeing the project progress related to the development of microdevices at CWRU.

Name: David Guggenmos
Project Role: Senior Investigator at KUMC
Researcher Identifier (e.g. ORCID ID): -
Nearest person month worked: -
Contribution to Project: Dr. Guggenmos coordinated the work at KUMC, including preparations for behavioral/surgical aspects of neurobiological studies, performing implantation procedures, troubleshooting neurophysiological equipment, and assisting in data analysis/interpretation.

Name: Caleb Dunham
Project Role: Research Analyst at KUMC
Researcher Identifier (e.g. ORCID ID): -
Nearest person month worked: -
Contribution to Project: Mr. Dunham was responsible for upgrading software and hardware platforms for neurophysiological data collection, creating data management systems, data analytic/processing tools, and storage related to neurophysiological data collected during experimentation.

Name: Heather Hudson
Project Role: Post-Doctoral Fellow at KUMC
Researcher Identifier (e.g. ORCID ID): -
Nearest person month worked: -
Contribution to Project: Dr. Hudson performed tasks related to assessing and validating functionality of rodent microdevices, assisting with development of the IACUC protocol, behavioral training, surgical procedures and post-operative behavioral assessment and analysis.

Has there been a change in the active other support of the PD/PI(s) or senior/key personnel since the last reporting period?

Nothing to report.

What other organizations were involved as partners?

Organization Name: University of Kansas Medical Center
Location of Organization: Kansas City, KS, USA
Partner's contribution to the project: Collaboration

8. SPECIAL REPORTING REQUIREMENTS

COLLABORATIVE AWARDS:

QUAD CHARTS:

9. APPENDICES:

Appendix I N. H. Vitale, M. Azin, and P. Mohseni, "A Bluetooth Low Energy (BLE)-enabled wireless link for bidirectional communications with a neural microsystem," in *Proc. IEEE Biomed. Circ. Syst. Conf. (BioCAS)*, pp. 371-374, Cleveland, OH, October 17-19, 2018 **(Selected for presentation in *Live Demonstrations* session)**.

A Bluetooth Low Energy (BLE)-enabled Wireless Link for Bidirectional Communications with a Neural Microsystem

Nicholas H. Vitale, Meysam Azin, and Pedram Mohseni

Electrical Engineering and Computer Science Dept, Case Western Reserve University, Cleveland, OH, USA
{pedram.mohseni@case.edu}

***Abstract*—This paper reports on the design and implementation of a Bluetooth low energy (BLE)-enabled wireless link for bidirectional communications between a user base station (UBS) and a neural microsystem. The microsystem comprises a previously developed application-specific integrated circuit (ASIC) for activity-dependent intracortical microstimulation (ICMS), and the BLE link is dedicated to remote programming of the ICMS ASIC as well as to remote monitoring of several parameters such as the average stimulus rate, electrode site impedance, or power supply level. A prototype system is developed that incorporates the ICMS ASIC, SAMB11 BLE module, and peripheral electronics for supply management and ASIC monitoring, as well as a BLE user interface custom developed in C#. The end-to-end functionality of the BLE-enabled wireless link is experimentally demonstrated in representative benchtop tests in which several ASIC parameters are successfully programmed from the UBS over a distance of > 3.5m. The prototype system consumes ~618µW from a 3.6V, 1.6Ah, lithium-ion battery and is estimated to feature a lifetime of > 8 months for continuous operation, making it suitable for longitudinal studies with the ICMS ASIC in a non-human primate model.**

***Index Terms*–Activity-dependent stimulation, Bluetooth low energy, brain-machine interface, intracortical microstimulation, neural microsystem, wireless communications.**

I. Introduction

Activity-dependent stimulation is an emerging approach in neural interfacing for creating artificial connections in the nervous system that can be used to re-establish lost sensory-motor communication channels in the cortex [1], or to regulate the neurochemical levels in the brain [2]. Specifically, in the electrical paradigm, such approaches have been employed to induce functional reorganization by driving Hebbian plasticity-based mechanisms in an injured nervous system [1], [3].

We have previously developed an application-specific integrated circuit (ASIC) for activity-dependent intracortical microstimulation (ICMS) that was capable of performing spike-triggered ICMS in the brain of an ambulatory rat [4], [5]. In longitudinal studies over the span of one month, the ICMS ASIC was successfully shown to facilitate rapid and significant recovery of the motor function in a skilled reach task involving rodent models of focal traumatic brain injury (TBI) in the caudal forelimb area (equivalent to the primary motor cortex) [1].

This work was supported by the Office of the Assistant Secretary of Defense for Health Affairs through the Joint Warfighter Medical Research Program under Award No. W81XWH-16-1-0503. Opinions, interpretations, conclusions and recommendations are those of the authors and are not necessarily endorsed by the Department of Defense.

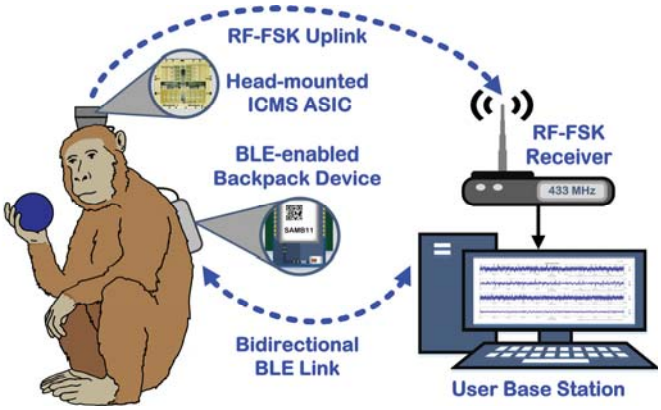

Fig. 1. Illustration of an experimental setup involving a non-human primate equipped with BLE-enabled backpack device for bidirectional wireless communications b/w head-mounted neural microsystem and user base station.

The next step in the evolution of this approach is to demonstrate the efficacy of activity-dependent stimulation in driving motor function recovery in a non-human primate model of TBI. However, such an effort is currently hindered by the lack of a bidirectional wireless communication link between the ICMS ASIC and a user base station (UBS). Specifically, while the ICMS ASIC does incorporate a radio-frequency frequency-shift-keyed (RF-FSK) transmitter operating at ~433MHz for wirelessly transmitting the neural activity on a selected channel to the UBS via the uplink [5], programming various ASIC parameters or temporarily monitoring the ASIC operation can only be done via a wired link from the UBS.

While this strategy was feasible in rodent experiments [1], [4], due to the ease of accessing the head-mounted system for connecting the wired link on a temporary basis, this approach would not work well in experiments with non-human primates in which the head-mounted system is typically enclosed within a skull-affixed primate chamber, making it impractical to use a wired link for programming the ICMS ASIC or monitoring its function during longitudinal studies, except sporadically for simultaneous multichannel monitoring of neural activity from the ICMS ASIC to assess recording quality.

In this work, we address this limitation by developing a low-power, bidirectional, wireless communication link between the head-mounted ICMS ASIC and the UBS using Bluetooth low energy (BLE), an emerging technology for biomedical applications [6]. Figure 1 illustrates an experimental setup involving a non-human primate equipped with the ICMS ASIC as part of a head-mounted device enclosed within a primate chamber, as well as a backpack device that contains a BLE module for bidirectional wireless communications with the UBS.

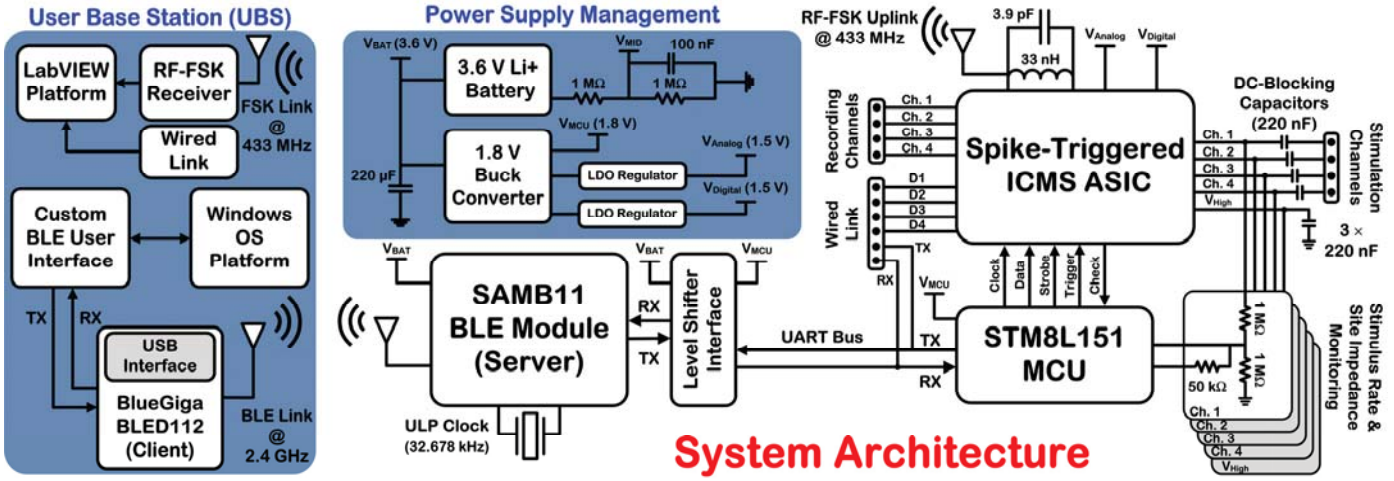

Fig. 2. System architecture for the implementation of a BLE-enabled, bidirectional, wireless communication link between the ICMS ASIC and the user base station.

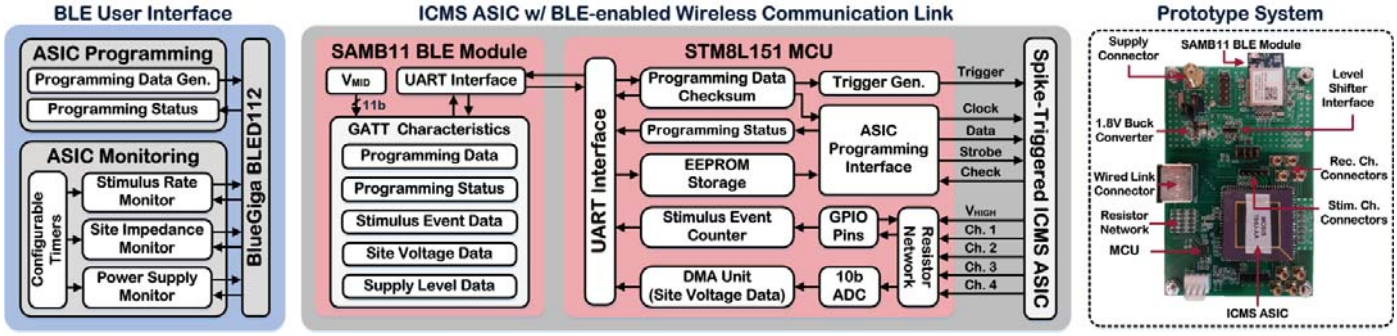

Fig. 3. **Left –** Illustration of the communication flow between the custom BLE user interface in the user base station and the ICMS ASIC. **Right –** Photograph of the system prototype, incorporating the ICMS ASIC, SAMB11 BLE module, and all requisite peripheral hardware.

II. BLE-ENABLED WIRELESS LINK DESIGN

A. *System Architecture*

Figure 2 depicts the system architecture for the implementation of the BLE-enabled, bidirectional, wireless communication link with the ICMS ASIC. The system can be partitioned into three separate sub-systems, namely, a UBS, a BLE module (SAMB11, *Atmel*) and power supply management electronics that are housed in the backpack device, and the ICMS ASIC and a microcontroller unit (MCU, STM8L151G6U6, *STMicroelectronics*) that are housed in the head-mounted device.

The UBS hosts a BLE user interface that is custom developed in C# for a Windows-based operating system (OS). This interface serves as a client-side console through which the user can initiate various BLE tasks for bidirectional communications with the ASIC using a universal serial bus BLE dongle (BlueGiga BLED112, *Silicon Labs*). Moreover, the UBS houses a LabVIEW-based platform that can receive and process neural signals recorded on one channel of the ASIC through the RF-FSK uplink at ~433MHz that is integrated onto the ASIC. If neural signals from all four channels of the ASIC are to be monitored simultaneously, a custom, wired, serial link can be utilized to communicate between the ASIC and the LabVIEW platform of the UBS on a temporary and sporadic basis.

The backpack device contains the BLE module, which serves as an intermediary data server between the UBS and the ASIC. Various tasks that require communications with the ASIC are commanded by the SAMB11 BLE module to the MCU via a universal asynchronous receiver-transmitter (UART) bus after bidirectional level shifting between 3.6V and 1.8V. The backpack device also contains the power supply management electronics, including a lithium-ion battery that directly powers the BLE module and a 1.8V buck converter that powers the low-power MCU. The buck converter also powers two low-drop-out (LDO) regulators that generate the 1.5V analog and digital supplies of the ASIC. Finally, a resistive voltage divider generates a reference voltage, V_{MID}, which is used for power supply level monitoring via the SAMB11 BLE module.

Finally, the head-mounted device contains the ICMS ASIC, low-power MCU, and the two LDOs for generating the ASIC power supplies. Utilizing the bidirectional nature of the BLE link, the system is designed to feature stimulus rate and site impedance monitoring for reporting back to the UBS upon user demand. Specifically, a resistive network is connected to each stimulation channel of the ASIC (and to its "high" voltage output of 5V) to attenuate the stimulus signal and meet the voltage level requirements of the general-purpose input-output (GPIO) pins of the MCU for stimulus rate monitoring, as well as the input level requirements of an analog-to-digital converter (ADC) integrated onto the MCU for site impedance monitoring.

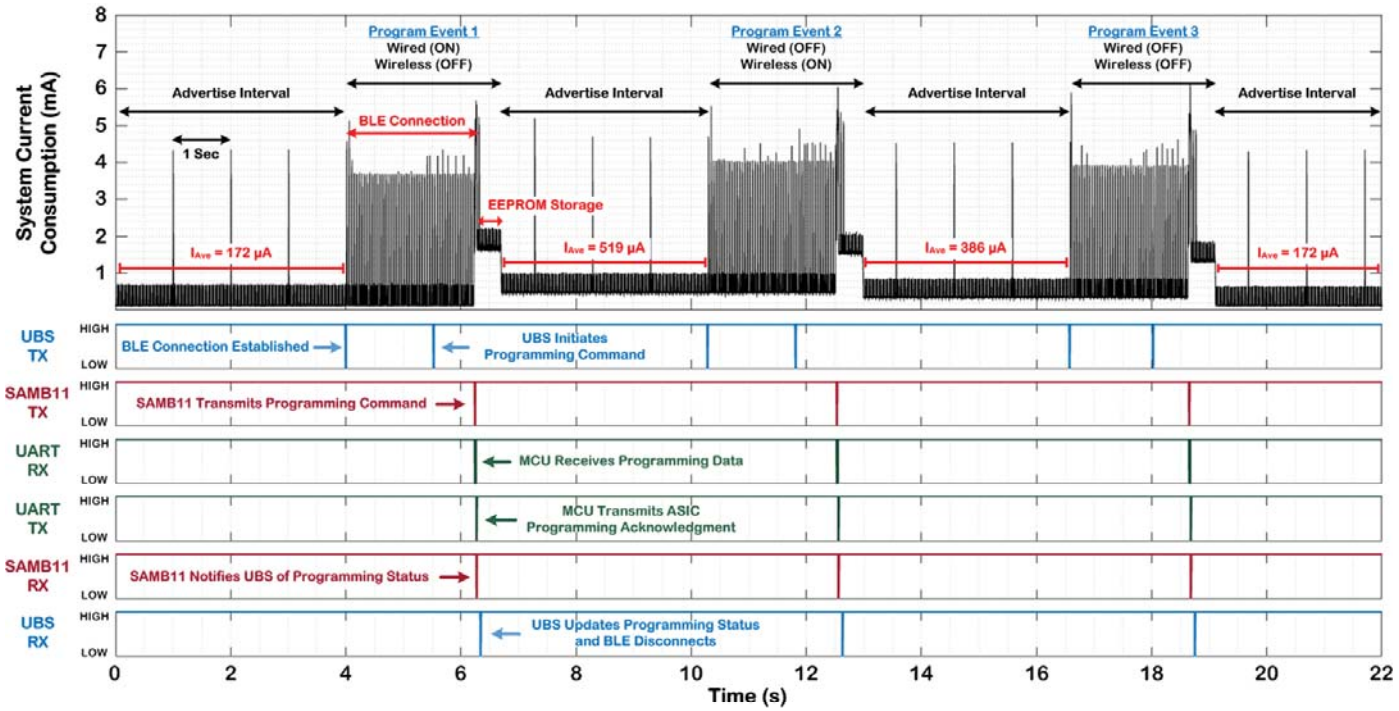

Fig. 4. Measured signals in various phases of system operation during BLE-enabled wireless ASIC programming from the user base station, resulting in successful toggling of ASIC operation between the wired and RF-FSK wireless modes, as reflected in the measured instantaneous system current consumption.

B. Communication Flow

Figure 3 illustrates the communication flow between the BLE user interface of the UBS and the ICMS ASIC for both programming and monitoring purposes. For all operations, the data received by the SAMB11 BLE module are stored within custom generic-attribute (GATT) characteristics. For ASIC programming purposes, 95 bytes of data are generated on the UBS and transmitted to the BLE module, containing the settings for the analog and digital blocks of the ASIC (92 bytes), as well as the setting for the source of stimulus trigger (3 bytes). The trigger source can be derived either in an activity-dependent manner from the ASIC itself (closed-loop) or via a *Trigger* signal from the MCU (open-loop). A simple checksum routine is preformed when the programming data are received by the MCU. If valid, the MCU will configure the trigger source and program the ASIC via the programming interface comprised of *Clock*, *Data*, and *Strobe* signals. In return, the ASIC sends back to the MCU an acknowledgment via a *Check* signal as the programming status, which is subsequently transmitted to the BLE module for notifying the UBS. If programming is successful, the MCU will save the programming data to its EEPROM for ASIC boot-up programming. Otherwise, the UBS is notified of the failure, and the MCU will skip over the EEPROM routine.

For ASIC monitoring purposes, the UBS receives information such as the average stimulus rate, electrode site impedance, and power supply level. These monitors can be set to execute on command or poll periodically by utilizing configurable timers located on the UBS. Specifically, the average stimulus rate per channel is monitored by counting the number of stimulation events within a pre-specified time window tracked by the UBS timers. The electrode site impedance is monitored by recording the corresponding site voltage waveform (and that of the "high" voltage output of the ASIC) using the 10b ADC of the MCU and transmitting the information to the UBS via the BLE module. A custom script on the UBS next analyzes the waveforms to evaluate the level of the site impedance. Finally, the supply level is monitored by averaging 256 samples of V_{MID} that are digitized with the 11b ADC of the BLE module and transmitting the results back to the UBS. Custom alerts can be created on the UBS to notify the user when supply level reaches a pre-specified critical value.

III. Measurement Results

To verify the functionality of the BLE-enabled wireless link in remote programming the ASIC functions from the UBS, representative benchtop tests were performed in which the ASIC was initially configured in its normal operating mode for stimulating on all four channels at a stimulus rate of ~33Hz and current level of ~40µA. Additionally, the wired and RF-FSK wireless links of the ASIC were disabled under the normal operating mode.

In our first experiment, programming data were compiled on and commanded from the UBS to remotely turn ON/OFF the wired and wireless links of the ASIC via the BLE module. Figure 4 shows the measured signals in various phases of the system operation that are time-synchronized with the measured instantaneous system current (in mA).

Prior to the first programming event, the wired and wireless links of the ASIC were disabled, as stated previously, and the BLE module was configured to advertise its identification information once every second. This can be clearly seen in Fig. 4 by the three large current peaks of ~4.4mA occurring once every second. The measured average system current prior to the

first programming event was ~172µA in which the SAMB11 BLE module consumed 13.2µA during advertising and idle modes, whereas the buck converter and the level shifter consumed 155µA and 3.8µA, respectively.

For the first programming event (i.e., turn ON the ASIC wired link), the UBS first established a BLE connection and then initiated a programming command for the MCU via the BLE module. Once ASIC programming was performed successfully, an acknowledgment signal was sent by the MCU to the BLE module for relaying back to the UBS upon which the BLE connection was severed. As seen in Fig. 4, within the duration of this programming event (~2.68 sec), the system consumed an average of 764µA, 42.9% of which was due to the BLE module. Ultimately, upon the termination of this programming event, the measured average system current increased from the previous baseline of ~172µA to a new higher level of ~519µA, indicating successful engagement of the ASIC's wired link.

Next, for the second programming event, the ASIC wired and wireless links were turned OFF and ON, respectively. As seen in Fig. 4, the same sequence of events repeated shortly after t = 10 sec, which ultimately decreased the measured average system current by 133µA to ~386µA. A final programming event turned OFF both wired and wireless links of the ASIC, returning the average system current to the baseline level of ~172µA.

In our second experiment, the BLE-enabled wireless link was used to remotely change the stimulus current level of the ASIC from the UBS. As seen in Fig. 5, from the time that the UBS initiated the programming command, it took < 0.8 sec to successfully update the programming status back at the UBS, although it should be noted that the ASIC stimulus current changed (from a maximum level of 94µA to 46µA) almost instantaneously once the MCU received and validated the programming data from the UBS. Collectively, these tests established the overall functionality and fast response time of the BLE-enabled wireless link for remote ASIC programming.

Table I tabulates the power breakdown of the prototype system with a 3.6V, 1.6Ah, lithium-ion battery (LTC16M-S4, *Eagle-Picher*). The system consumed a total of 618.2µW during its normal operation mode, with the ASIC and the two LDOs consuming 405µW while the BLE module and the MCU consumed 71.6µW. The system lifetime for continuous operation in its normal mode was estimated to be > 8 months based on our battery lifetime tests, although this estimate is subject to change based on the rate of use of the wired/wireless links of the ASIC and the level of the output stimulus current. It should also be noted that the BLE transmission range in all aforementioned experiments was ~3.6 meters (i.e., 12 ft).

IV. Conclusion

This paper reported on the design and implementation of a bidirectional wireless communication link between a user base station and a neural microsystem using low-power BLE technology. A prototype system was developed that incorporated a SAMB11 BLE module, an activity-dependent ICMS ASIC, and peripheral electronics for supply management and ASIC monitoring. The system was successfully used to remotely program several ASIC parameters from the user base station over a distance of > 3.5m, while consuming ~618µW from a 3.6V, 1.6Ah, lithium-ion battery.

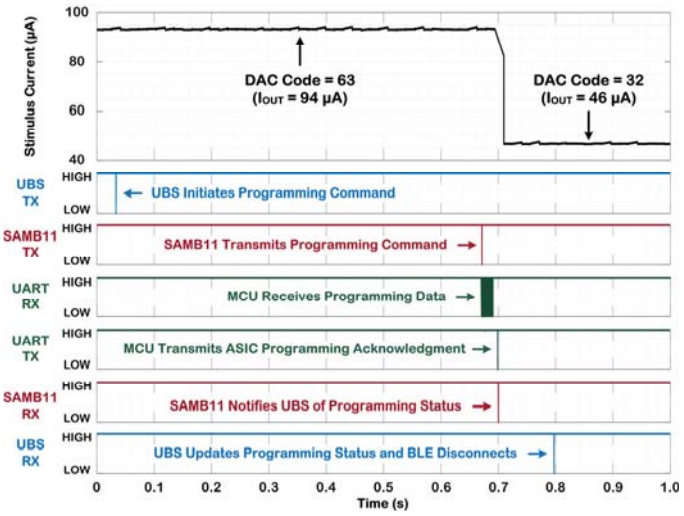

Fig. 5. Measured signals in various phases of system operation during BLE-enabled wireless ASIC programming from the user base station, resulting in successful re-programming of the ASIC stimulus current from maximum level of ~94µA to ~46µA.

TABLE I
SUMMARY OF POWER BREAKDOWN

Subsystem	Building Block	Power (µW)	%
Backpack Device	Level Shifter Interface	13.7	2.2
	SAMB11 BLE Module	47.5	7.7
	3.6V-to-1.8V Buck Converter Loss	127.9	20.7
Head-Mounted Device	MCU	24.1	3.9
	ASIC (Digital)	94.1	15.2
	1.5V LDO Loss (Digital Supply)	38.2	6.2
	ASIC (Analog)	233.7	37.8
	1.5V LDO Loss (Analog Supply)	39.0	6.3
Total System Power Consumption		**618.2**	**100**

References

[1] D. J. Guggenmos, et al., "Restoration of function after brain damage using a neural prosthesis," *Proc. Natl. Acad. Sci. USA (PNAS)*, vol. 110, no. 52, pp. 21177-21182, Dec. 2013.

[2] B. Bozorgzadeh, et al., "Neurochemostat: A neural interface SoC with integrated chemometrics for closed-loop regulation of brain dopamine," *IEEE Trans. Biomed. Circ. Syst.*, vol. 10, no. 3, pp. 654-667, Jun. 2016.

[3] J. G. McPherson, et al., "Targeted, activity-dependent spinal stimulation produces long-lasting motor recovery in chronic cervical spinal cord injury," *Proc. Natl. Acad. Sci. USA (PNAS)*, vol. 112, no. 39, pp. 12193-12198, 2015.

[4] M. Azin, et al., "A miniaturized system for spike-triggered intracortical microstimulation in an ambulatory rat," *IEEE Trans. Biomed. Eng.*, vol. 58, no. 9, pp. 2589-2597, Sep. 2011.

[5] M. Azin, et al., "A battery-powered activity-dependent intracortical microstimulation IC for brain-machine-brain interface," *IEEE J. Solid-State Circuits*, vol. 46, no. 4, pp. 731-745, Apr. 2011.

[6] S. K. Lin, et al., "A smart headband for epileptic seizure detection," in *Proc. IEEE Healthcare Innovations and Point-of-Care Tech.*, pp. 221-224, Nov. 2017.

Appendix II S. Barbay, H. Zhang, S. B. Frost, J. C. Peterso, D. J. Guggenmos, H. M. Hudson, D. T. Bundy, S. DeJong, and R. J. Nudo, "A cortical injury model in a non-human primate to assess execution of reach and grasp actions: Implications for recovery after traumatic brain injury," *under preparation for submission*.

A Cortical Injury Model in a Non-Human Primate to Assess Execution of Reach and Grasp Actions: Implications for Recovery after Traumatic Brain Injury

Scott Barbay PhD[a], Hongyu Zhang MD, PhD[a], Shawn B. Frost PhD[a], Jeremy C. Peterson MD[b], David J. Guggenmos PhD[a], Heather M. Hudson PhD[a], David T. Bundy PhD[a], Stacey DeJong PT, PhD, PCS[c†], and Randolph J. Nudo PhD[a,c]

a. University of Kansas Medical Center, Dept. of Physical Medicine and Rehabilitation
b. University of Kansas Medical Center, Dept. of Neurosurgery
c. University of Kansas Medical Center, Landon Center on Aging
†. Permanent address: University of Iowa, Carver College of Medicine, Department of Physical Therapy and Rehabilitation Science

Corresponding Author:
Scott Barbay PhD
Cortical Plasticity Laboratory
Dept. of Physical Medicine and Rehabilitation
University of Kansas Medical Center
Kansas City, KS 66160
Telephone: 913-588-9911
Fax: 913-945-6827
Email: sbarbay@kumc.edu

Running Title: Recovery from Traumatic Brain Injury

Abstract

Background: Technological advances in developing experimentally controlled models of traumatic brain injury (TBI) are prevalent in rodent models and these models have proven invaluable in characterizing temporal changes in brain and behavior after trauma. To date no long-term studies in non-human primates (NHPs) have been published using an experimentally controlled impact device to follow behavioral performance over time.

New Method: We have employed a controlled cortical impact (CCI) device to create a focal contusion to the hand area in primary motor cortex (M1) of three New World monkeys to characterize changes in reach and grasp function assessed for 3 months after the injury.

Results: The CCI injury destroyed ~79% of the M1 hand representation (73.6%,76.7% and 85.6%, respectively) and ~9% of the underlying corona radiata (5.29%, 4.1% and 11.66%, respectively). Impaired motor function was confined to the hand contralateral to the injured hemisphere. Typical non-volitional hand activity was only transiently affected during the first few days after injury while skilled hand grip was impaired over three months of observation.

Comparison with Existing Method(s): This study is unique in establishing a CCI model of TBI in a NHP resulting in persistent impairments in motor function evident in volitional use of the hand.

Conclusions: Establishing an NHP model of TBI is essential to extend current rodent models to the complex neural architecture of the primate brain. Moving forward this model can be used to investigate novel therapeutic interventions to improve or restore impaired motor function after trauma.

Acknowledgements: Supported by Department of Defense Award No. W81XWH-16-1-0503.

A Controlled Cortical Impact Injury Model in a Non-Human Primate to Assess Execution of Reach and Grasp Actions: Implications for Recovery after Traumatic Brain Injury

1.0 Introduction

Traumatic brain injury (TBI) is a major cause of death and disability. In 2014 the Centers for Disease Control and Prevention reported 2.53 million TBI-related injuries in the United States requiring 288,000 hospitalizations[1]. Because the number of TBI related deaths has decreased since 2001 due to advances made in acute management of TBI[2,3] many more TBI patients are surviving but with life-long disabilities. Efforts to improve daily lives of these patients are progressing by developing new translational models of TBI that focus on a variety of injury-related comorbidities. New studies are examining various aspects of TBI regarding initial severity and secondary outcomes such as neurodegeneration and delayed pathology related to cognitive and emotional aspects of TBI injury including an increase in studies assessing subsequent motor impairment. Variation in models range from global injuries to detect molecular disruption throughout the brain to more focal injury to assess memory or movement impairments as they apply to restorative therapies. Many investigators use focal injuries to reduce the range of complications of TBI with the intention of eventually addressing more generalized impairment with diffuse injury models[4,5]. One of the most common approaches for inducing focal impact injuries is the controlled cortical impact (CCI) model which allows reasonable consistency in the size and severity of injury[6]. However, to date, most CCI studies utilize rodent species, primarily rats and mice. As CCI injuries

have rarely been applied to larger animal models, it was our goal to extend this common focal injury approach to a non-human primate (NHP) species.

Most of the technical aspects for establishing parameters for reliable and valid implementation of experimental brain injury have been developed in rat models. Specifically, the Long Evans rat has been a reasonable model for these studies, and we have developed reliable methods for creating repeatable CCI injuries in motor cortex in this strain and have tested novel therapeutic approaches[15,16, Andrews et al 2020[17]]. However, rodents have limitations with regard to translation to clinical studies. As novel restorative therapies are emerging from the rodent literature,[7] development of addiitional translational models are needed to establish feasibility and efficacy in more complex mammalian nervous systems such as those of NHPs).[8-11] To date, CCI injury models in NHPs have only been established for short-term (< 2 days) survival studies.[32]

NHP models of brain injury are well suited to address multiple neural mechanisms capable of supporting recovery, providing a potential model for rehabilitative or restorative therapies[9,12-14]. As we have had several decades of experience with focal ischemic lesions in motor cortex of squirrel monkeys (Saimiri *spp.*), [18-28] the present study was designed to test the feasibility and reproducibility of CCI injuries in squirrel monkeys. An advantage of this species for initial characterization of this model is that the somatosensory and motor areas are easily accessible on a flat, relatively unfissured sector of frontal cortex. Also, squirrel monkeys have well developed parietal-frontal networks related to visuomotor control of the forelimb and hand mediated through several premotor cortical areas unique to primates[29]. The complex neurophysiological interaction within the visuomotor system of

primates, offers a unique flexibility of muscle recruitment to achieve behavioral goals[30] guiding the development of novel therapies that can later be tested in human cohorts. The present study is unique with regard to the long-term (3 months) assessment of motor recovery after a CCI injury in an NHP.

2.0 Methods

Three male squirrel monkeys (Saimiri *spp.*, weight range 828 – 1102g) were used to model a focal concussive injury restricted to the distal forelimb area (DFL) of primary motor cortex (M1). All procedures were conducted in accordance with institutional and federal guidelines for care and use of experimental animals and with approval from the Institutional Animal Care and Use Committee. Monkeys were housed in a climate-controlled vivarium. Food (Purina Lab Diet #5088) was provided twice daily (supplemented with fruit and vegetables) and water was provided *ad libitum* through an automatic watering system. On days when behavior was assessed, feeding was scheduled after assessment. Routine health checks were made daily by Laboratory Animal Resource staff under supervision of the institutional veterinary staff.

2.1 General Procedures.

Each monkey received a focal concussive injury after craniectomy over the M1 DFL using the CCI procedure in either the left or right hemisphere (contralateral to their preferred hand used on a dexterity task). The DFL area was delineated using standard intracortical microstimulation (ICMS) procedures to delineate proximal and distal forearm movements[18-28]. Behavioral assessments of dexterity and power grip were

obtained over five sessions distributed over two weeks prior to a CCI, and once per week over the following three months after injury. Neural recordings were acquired within and adjacent to the cortical impact area in two monkeys at the end of behavioral assessment in a final procedure to verify the effectiveness of the injury (3 months post-CCI). All monkeys were humanely euthanized at the end of the experiment followed by transcardial perfusion and fixation with 10% Formal saline.

2.1.1 Behavioral Procedures.

General methodology. Two different behavioral tasks were used to assess dexterity and hand grip performance, respectively (**Figure 1**). In both behavioral tasks, monkeys were reinforced with a food reward for successful performance. First, a modified Klüver board was used to determine hand preference, and to assess dexterity by presenting food-pellets to the monkeys on a flat manually rotated disk with wells of different size for placement of food pellets, as described in more detail below. Second, a hand grip device was used to assess complex and simple use of the power grip. The hand grip device was programmed to two different sets of criteria, providing the means to assess power grips on either a “Difficult Task” or an “Easy Task” as described below. To obtain a food reward, the monkey was required to squeeze a handle embedded with a calibrated force transducer, applying a target force range for a specified time. If the criteria were met for an individual grip, food-pellets were delivered to a food bin placed within the monkey’s cage once when the handle was released. Learning the association between gripping the handle and receiving a reward was more challenging for the monkeys than extracting food pellets from the food-wells, and thus required

multiple sessions for consistent performance.

Subsequent to learning each of the behavioral protocols, the behavioral tasks were presented to each monkey five days per week during single sessions in the order of most difficult to easiest task: “Difficult” hand grip task followed by the Klüver disk task and ending with the “Easy” hand grip task. This order was used to maintain motivation to work for food-pellets on each task. Pre-injury baseline performance was collected over five sessions. Natural recovery from injury was assessed beginning one week after the CCI injury and continuing once per week for 13 weeks. Behavioral assessments after injury were conducted weekly to minimize potential training effects. Behavioral sessions were videotaped for later analysis.

Klüver disk task. This task was slightly modified from one used in several of our previous publications[18-21] to accommodate the food wells on a circular disk (**Figure 1A**). A circular Plexiglas disk attached to a frame and mounted onto the front of the monkey’s home cage, with five food wells drilled into its surface. The frame incorporated a sliding door that restricted retrievals to the preferred hand both before and after injury. The disk could be rotated to present each food well to the same position in front of the monkey. Each well was 5 mm in depth and ranged in diameter from 25 mm to 9.5 mm (designated wells 1-5 respectively): Well-1 = 25 mm dia.; Well-2 = 19.5 mm dia.; Well-3 = 13 mm dia.; Well-4 = 11.5 mm dia.; Well-5 = 9.5 mm dia.. The Klüver disk task consisted of reaching through the cage bars, inserting one or more fingers into a food well, and retrieving a single, small banana flavored food pellet (45 mg; BioServe, Flemington NJ). Food pellets were placed one at a time into one of the five food wells in a randomized block design (i.e., equal number of presentations for each well).

Dexterity was measured as the number of digit flexions necessary to remove food pellets presented per well on each session. There were three steps to establishing baseline performance on the Klüver disk task: (1) acclimation/hand preference assessment; (2) skill training on all food-wells; and (3) random probe trials on all food-wells. Prior to training, each animal was acclimated to the Klüver disk and assessed for hand preference over 50 trials a day on two consecutive days while reaching and grasping food pellets with either hand without restriction. Hand preference was determined as the hand used for over 50% of the trials. Training was conducted with each animal's preferred hand over ten consecutive days for 30 min per day beginning with the largest well (Well-1) and ending with the smallest well (Well-5) on the 10^{th} day. Wells 4 and 5 had the smallest diameter and were the most difficult for the monkeys to extract the food-pellets. To encourage motivation, a progressive training schedule was instituted. The timeline for training on the Klüver disk was as follows: Day 1: Well-1; Day 2: Well-2; Day 3: Well-3; Day 4: 50% Well-3/50% Well-4; Day 5: Well-4; Day-6: 50% Well-4/50% Well-5; Day-7 through Day-10: Well-5. Probe trials were used to maintain performance while training began with the grip-tasks (see methods below). The probe trial session consisted of randomly presenting 10 food-pellets per well to each animal's preferred hand. Baseline performance was based on the last five sessions prior to CCI.

Hand-grip task. The grip device consisted of an aluminum cylinder connected to a universal joint allowing the cylinder to rotate in multiple directions (**Figure 1B**)[31]. The cylinder and u-joint (grip handle) were attached to an aluminum frame mounted to the monkey's home cage, suspending the grip handle in front of the monkey. The grip

handle was attached to a rail running along the length of the frame and could be adjusted to each monkey's hand preference. A sliding Plexiglas door was used to limit the monkey to use of either the left or right hand based on hand preference on the Klüver task. The combination of the u-joint and the sliding grip handle helped to minimize the use of proximal musculature during the power grip[31]. Grip force was measured by a Honeywell Sensotec Compression Load Cell with a 1,000 g limit and 0.01 g resolution (Honeywell Sensotech, Columbus Ohio). The load sensor was checked for calibration prior to each session. The grip task required each monkey to exert and hold a grip force between a low and high cutoff point over a specified period of time to receive a food pellet reward. A LabView program was used to acquire grip information and set parameters used to assign successful grip instructions necessary to achieve a food reward. Training began with an initial reward criterion of 25 to 500 g force for 0.5 sec. Training proceeded by increasing the lower limits of grip force while lowering the upper limits in increments of 25 g while increasing hold time by 0.5 sec. When 60 pellets were obtained, the reward thresholds were changed until the monkey could attain 100 – 300 g force for 3 sec. To obtain a food reward, the monkey was required to squeeze the handle activating a force transducer, applying a specified range of force and time defined for the "Difficult" and "Easy" task. Food-pellets were delivered to a food bin placed within the monkey's cage once the handle was released. The monkey could make as many grips as possible during a 30-min session on the "Difficult" task and during a 5-min session on the "Easy" task.

2.1.2 Data analysis.

Hand dexterity was assessed as the number of digit flexions necessary to retrieve food pellets from the Klüver disk. Grip performance was assessed as the number of successful grips made during a 30-min session on the "Difficult" task and during a 5-min session on the "Easy" task. Each monkey's individual performance score on a given day was compared to that monkey's distribution of pre-injury baseline performance over five sessions. Each monkey's average baseline success and standard deviation was used to establish a 95% confidence interval (Z = 1.95) used to determine a significant deviation from pre-injury baseline performance.

Insert **Figure 1** here.

2.2.0 Surgical Procedure.

Sterile surgical procedures were used to expose the M1 DFL and the surrounding cortical territory to identify movement representations as defined by ICMS techniques. Monkeys were sedated with an initial dose of ketamine (20 - 30 mg/kg, i.m.) followed by atropine (0.07mg/kg i.m.). Supplemental doses of ketamine (20 – 30 mg/kg i.m.) were administered as needed as the monkeys were weighed and examined in preparation for the surgical procedure. The scalp, forelimb (opposite the cerebral hemisphere to be mapped) and hindlimb (for catheterization) were shaved and cleaned. The trachea was treated with a 20% benzocaine spray followed by 2% lidocaine jelly while intubated (2.5-3.0 mm i.d. tracheal tube). Following surgical preparation, isoflurane (0.5 to 3%) was introduced and the saphenous vein catheterized with a 24-gauge angiocath for delivery of lactated Ringers with 3% dextrose (10ml/kg/hr) and

other required fluids. Ophthalmic ointment was liberally applied to the corneas and the monkey was placed into a stereotaxic frame. The incision area was infiltrated with 0.5% bupivacaine (1 ml s.c.) and scrubbed with alcohol and iodine. Penicillin-G benzathine + procaine (45K IU, s.c.), dexamethasone (0.50mg i.v.) and mannitol (2g/kg i.v.) were administered.

Under aseptic conditions and 1.5% – 3% isoflurane- 75% nitrous oxide anesthesia, a craniectomy (~1.5 cm^2) was performed over M1 and extended to include S1 and premotor cortex contralateral to the monkey's preferred hand. A sterile plastic chamber was temporarily secured over the opening and filled with sterile silicone oil to protect the cortex during the ICMS procedure and removed prior to the CCI procedure. Inhalation anesthesia was withdrawn, and ketamine (5mg dose), supplemented by diazepam (0.01mg per dose), was administered intravenously as needed. Vital signs were monitored and maintained within normal limits throughout the procedure. Heart rate, saturated oxygen, respiration rate and expired CO_2 were monitored with a gas monitoring system and core body temperature was monitored and maintained with a homothermic blanket system. Following an ICMS mapping procedure identifying DFL (see below), inhalation anesthesia was reinstated, and the dura replaced over the cortex. A CCI was then delivered (see below). The dura was then removed and replaced with a thin silicone sheet. Dental acrylic was used to replace the craniectomized bone over M1, and the incision was sutured and treated with 0.5% bupivacaine (1ml s.c.).

Post-operative support included penicillin-G benzathine + procaine (45K IU, s.c.), topical triple antibiotic and analgesics acetaminophen (10-20 mg/kg) /codeine (1 – 2

mg/kg) solution (oral) and tramadol (3 mg/kg, i.m.). Supplemental support was given as needed determined by veterinary consultation. Monkeys were monitored in a temperature-controlled incubator until recovery from anesthesia was complete and the animal was alert and stable (indicated by mobility, eating/drinking, waste elimination), and then returned to their home cages. Prolonged care procedures included wound care as needed, suture removal at ~2 weeks post-surgery and daily monitoring of general health[26].

A final surgical procedure was performed as described above at the experimental end point (3 months post-CCI) to assess damage to cortex within and around the impact. A digital photomicrograph was taken of the cortical surface and used to assess extent of the cortical damage. Neural recordings were acquired within the M1 infarct area and in the adjacent premotor cortex. Monkeys were humanely euthanized at the end of the final procedure.

2.1.3 ICMS Procedure.

A cortical mapping procedure was used to identify the distal forelimb representation (digits, wrist and forearm) and its borders with the proximal forelimb (shoulder, elbow) and face representations. Movements were evoked by delivering electrical current through a stimulating microelectrode (~15 μm tip o.d.) placed perpendicularly to the cortical surface, targeting layer V at a depth of ~ 1750 μm. The microelectrode consisted of a platinum wire insulated by a glass micropipette filled with a 3.5 M NaCl solution. Current was delivered from a BAK stimulus isolator (Model BSI-2, BAK Electronics Inc.) as a 45 msec pulse train consisting of 13 cathodal monophasic

pulses (0.2 ms duration; 3.3 ms between pulses; capacitively coupled), with pulse trains delivered once per sec. The stimulus pulse was programed via a Master-8 stimulus pulse generator (A.M.P.I., Isreal), and the current waveform was monitored on an oscilloscope. Maximum current did not exceed 30 μA.

2.1.4 CCI Procedure.

A commercial electromagnetic impact device was used to deliver a traumatic brain injury to the M1 DFL (Impact One, Leica Biosystems, Buffalo Grove, IL). Parameters for the CCI were entered into a control unit attached to a linear actuator mounted on a micropositioner. The arm of the micropositioner was modified with a universal joint to align the impact tip perpendicular to the cortical surface. Conductance through the impact tip allowed calculation for the depth of impact from the surface of the cortex. The impact parameters were based on previous studies using CCI procedures [16, 32, 33]. The impact tip was a stainless-steel rod with a 5 mm diameter tip (slightly beveled to remove sharp edges around the perimeter). The impact tip was aligned over the center of the M1 DFL as delineated with ICMS and recorded onto a photomicrograph of the cortical surface. The boundary of the DFL was aligned relative to the surface blood vessels. The impact was delivered with a depth of 3 mm from the cortical surface, at 4.5 m/sec with a dwell time of 200 msec.

2.1.5 Neurophysiological Procedure.

In 2 of the 3 monkeys, neural recordings were collected three months after CCI under 1% isoflurane anesthesia to assess effectiveness of the injury. A single shank

Michigan electrode with 16 independent recording sites spaced vertically, 100 μm apart along the shank (NeuroNexus, Ann Arbor MI) was inserted at a depth of 1700 μm below the surface of the cortex. Spontaneous neural activity was sampled at three sites within the DFL impact area and three sites in the peri-infarct area anterior and posterior to the DFL. Each site was sampled continuously for 5 min. Neural activity was amplified and sorted with a 32 channel Tucker-Davis Technology's (TDT) RZ50 neurophysiology system (Tucker-Davis Technology's, Alachua, FI).

We also recorded within somatosensory cortex (S1) to delineate the cutaneous representations of digits 1 and 2 for reference. A Michigan-style electrode (NeuroNexus, Ann Arbor, MI) was lowered perpendicular to the cortical surface to span cortical layers II-V. Signals were filtered and amplified using a commercial neurophysiological recording system (Tucker Davis Technologies, Alchula, FL) and played over a loudspeaker for monitoring. Receptive fields were determined by neural responses in S1 to light touch with a Semmes-Weinstein monofilament 3.61 (~400 mg force).

2.1.6 Histological Procedure.

Monkeys were humanely euthanized with a combination of dexdormitor 100 mcg/kg i.m. followed by Beuthanasia-D 1.5 cc i.p. The animals were then perfused through the left ventricle of the heart with heparinized saline and lidocaine followed by 10% Formal saline.

Analysis of injury extent on cortical surface. Pre- and post-CCI digital photographs of the cerebral cortex were compared to identify the lesion area. Pre-CCI

cortical maps showing location of the M1 DFL area targeted for impact were superimposed onto the digital photograph of the cerebral cortex. This composite photograph with functional boundaries was compared to a digital photograph of the post-CCI cortical surface, and a graphics program (Canvas v12, ACD Systems of America) was used to measure the cortical extent of the lesion in mm^2. Changes in cortical surface area were identified relative to changes in blood vessel patterns and necrotic tissue[27]. Whole brains were fixed in 10% formalin and stored in 0.1 M sodium phosphate buffered saline (PBS) and then shipped to Neuroscience Associates (NSA, Knoxville Tenn.) for histological processing. Coronal sections were cut at 40 μm thickness. In each animal, we used 42 Weil stained sections (80 μm separation between sections) through the impact area (5 mm) and adjacent tissue to evaluate the change of volume limited to the corona radiata. The contour of gray matter, white matter and the injured boundaries in each section were visualized with the Weil stain and traced under 2.5X magnification using a quantitative microscopy system (Neurolucida; MBF-Bioscience version 11). The volumes of the corona radiata under the impact area of cortex in injured and intact hemispheres were estimated according to the Cavalieri principle using the section cut thickness (40 μm), a slice interval of 3, and a 400 μm grid spacing (StereoInvestigator, MBF-Bioscience, Version 11).

3.0 Results

3.1.0 Lesion Extent.

In each of the three monkeys, the cortical territory at the site of impact appeared shrunken three months after the CCI (**Figure 2B**) that was clearly visible as a necrotic area in the perfused brain (**Figure 2A**). Comparison of pre-CCI and three-month post-CCI photographic images revealed a reduction in impacted M1 DFL cortex for each monkey exceeding 70% of the impacted area: 73.6%, 76.7% and 85.6% in A401, A385 and A413, respectively (**Figure 3B**). Myelin-stained sections show that in each of the three monkeys, the lesion was almost exclusively confined to the cortical grey matter, with minimal to no intrusion into the underlying white matter (**Figure 3C**). Estimated volume of white matter within the corona radiata beneath M1 DFL indicated a small loss of fibers in each monkey. The volume of corona radiata underlying the injured cortex was reduced by 5.29%, 4.10%, and 11.66% in A401, A385 and A413, respectively.

[Insert **Figure 2** here.]

Neural recordings were collected within, and adjacent to, the impact area to compare spiking activity in the targeted M1 DFL and in adjacent perilesion areas anterior and posterior to the impact (**Figure 2B, C**). Neural activity within within the impact zone showed less spontaneous spiking activity than tissue outside the area of impact.

[Insert **Figure 3** here.]

3.2.0 Behavioral Assessment on Klüver Disk Task.

The ability to successfully reach and retrieve pellets from each of the five food-wells varied among the three monkeys after the CCI injury (**Figure 4**). Two of the three monkeys (A413 and A401) could not successfully retrieve a food pellet from any of the wells initially after the CCI. A413 was able to retrieve pellets from well 4 by the by the second week after the injury but could not retrieve from well 5 (smallest well) until 7 weeks after the injury. A401 was able to perform the task on wells 4 and 5 by the third week after the injury. Difficulty in grasping and retrieving food pellets from the food-wells persisted as indicated by the number of finger flexions required to extract and retrieve a food pellet. Impairment in extracting food pellets lasted through the entire three months of post-CCI assessment. Even though extracting the food pellets from the larger food wells (wells 1 to 3) was affected by the impact, all monkeys could extract food pellets with one or two flexions by the third week (well 1-3 data not shown). Impaired motor skills were more pronounced for extracting food pellets from the smallest wells (well 4 and well 5).

[Insert **Figure 4** here.]

3.3.0 Behavioral Assessment on Hand Grip Task (**Figure 5**).

Easy task (25 – 500 g for 0.5 sec). Prior to the CCI injury, each of the three monkeys was able to perform the Easy task. However, there was substantial session-to-session variability in the number of successful grips, especially in A413. After the injury, each of the three monkeys was able to perform the Easy grip task throughout the post-injury period. However, the number of successful grips per session occasionally fell below the pre-lesion baseline range (> 2 std dev). Significantly fewer successful

grips were observed for A413 on post-injury week 2, A385 on week 1, and A401 on week 7.

Difficult task (100 – 300 g for 3 sec). Prior to the CCI injury, each of the three monkeys was able to perform the Difficult grip task, which required a more restricted force range for an extended time period compared with the Easy task. Prior to CCI injury, task acquisition varied among the three monkeys learning to hold a grip between 100 – 300 g for 3 sec: A401 required 50 sessions, A413 required 46 sessions and A385 required 35 sessions. Performance on the Difficult grip task also varied among the three monkeys after CCI injury. During the first week after CCI each of the monkeys had difficulty reaching the 100 g threshold and maintaining a grip between 100 and 300 g for 3 sec. Each of the monkeys were able to within the baseline range (95% CI of their respective baseline performance) within 5 weeks. However, performance of A385 was highly variable and declined by week 6 relative to baseline. Grip performance in this animal generally remained below baseline levels through the remainder of the 13 week study. The other two monkeys (A401 and A413) remained within their 95% CI from week-6 to week-13 and performing consistently within the baseline range by the end of the study.

[Insert **Figure 5** here.]

4.0 Discussion

Over the last few decades, the intrinsic capacity of the mammalian brain to reorganize after injury and restore motor function has been demonstrated with various

animal models[34-36]. Translational research identifying adaptive molecular mechanisms initiated by injury and subsequent anatomical reorganization are leading to new innovative therapies to restore neurological function[35]. A major benefit of using animal models is the control of variability in size and location of injury to address specific mechanisms underlying consequential neuropathology and recovery[36]. This depends upon controlling the specificity of a brain injury to isolate the contribution of distinct neural systems in the development of subsequent anatomical and physiological disruption and potential resolution of function (e.g., cognitive, motivational and motor). Improvements in cortical impact devices such as the programmable CCI impactors currently in extensive use have allowed for necessary experimental control to examine various aspects of traumatic brain injury[33]. Choosing the most appropriate species is also necessary when assessing reorganization of complex neural systems and behavioral outcomes. In this study we present an NHP model of TBI to assess deficits in motor performance and ultimately, subsequent changes in functional neural connectivity responsible for the recovery. The evolution of cortical specializations in primates results in unique sensorimotor integration patterns between anatomically separated cortical areas necessary for the complex behavioral demands of their environments[37,38].

This initial study to introduce an NHP model of TBI focuses on motor recovery in the use of the forelimb, characterized disruption of grasping performance during natural recovery from a CCI injury to the DFL (including the hand) representation in M1. We chose a focal M1 injury for our initial study because of the multiple corticocortical loops with premotor (PMv, PMd, SMA), somatosensory and parietal cortices, contributing to

the complexities of motor control of skilled use of the hand, and because of the wealth of data from our laboratory on the effects of ischemic infarcts in M1. In primates, multiple hand areas exist in remote locations within motor and sensory cortex. Each hand area in premotor and somatosensory cortex communicates directly with M1[38-40]. Injury to one or more specialized hand areas such as M1, ventral premotor cortex, dorsal premotor cortex or the supplementary motor area, leads to reorganization of activity within areas not directly injured and this reorganization is associated with behavioral recovery[24,25,41].

In the present study, an impact confined to the DFL representation of M1 in squirrel monkeys impaired volitional, goal directed movements requiring skillful manipulation of digits and sustained grip. Typical behaviors such as feeding, grooming, and arboreal locomotion were only transiently affected contralateral to the CCI, recovering within the first week of injury. This is similar to what we have seen after a focal ischemic infarct to the M1 DFL in this species[22]. Throughout the following weeks of recovery after the CCI, moderate motor impairments were observed during performance on two tasks that required skilled use of the distal forelimb learned prior to injury. Thus, in general, the CCI model was quite successful in the squirrel monkey, using impact parameters similar to those used in rodents. Effective lesions of similar size were produced, and the injuries resulted in moderate motor impairments. Also, the damage wwas largely confined to the cortex with minimal damage to the underlying white matter.

The Klüver disk task required squirrel monkeys to retrieve food pellets from various sized food-wells, usually by bracing some of their digits or palm against a Plexiglas board while manipulating a small food pellet with their free digits. This is a

learned motor skill for squirrel monkeys[21]. With practice, uninjured monkeys can learn to retrieve food pellets with a single flexion from the smallest food well. After ischemic injury to motor cortex, the number of digit flexions needed to remove a food pellet increases[22]. Cortical injury associated with CCI were also persistent and more severe than motor impairments seen after an ischemic injury. Some improvement in skilled use of digits improved naturally over time (i.e., spontaneously or without rehabilitative training) but in two of the three monkeys (A413 and A385), grasping performance was still well below pre-injury baseline levels after 13 weeks of post-CCI assessment. Monkey A401 performed the Klüver disk task better than monkeys A413 and A385 prior to injury and showed better recovery over time. It is worth noting that this monkey also had the smallest lesion of the three monkeys.

The persistent impairment affecting coordinated use of digits during pellet retrieval is similar to those reported with patients diagnosed with pure motor hemiparesis as the monkeys were able to regain use of hand and digits but not fully recover function needed for skilled motor performance[42]. Typically, clinically identified pure motor hemiparesis is seen after lacunar stroke in the posterior limb of internal capsule, corona radiata, or corticospinal tract. Lang and Scheiber found that damage restricted to motor cortex and corticospinal tract would also result in a pure motor hemiparesis of the hand affecting finger movements but not cognitive aspects of movement[42].

Impaired use of the hand was also evident from the sustained grip task we implemented within a conditional association paradigm. The monkeys had to associate their grip with a food reward located at a distance from the grip handle under specific

conditions defining the force and duration of the grip. The injury resulted in a less severe or transient impairment in gripping behavior in contrast to grasping behavior observed on the Klüver task. The ability to sustain a power grip between 100 to 300 g of force for 3 sec ("Difficult Task") recovered to baseline for each monkey. Grip performance in two of the monkeys (A413 and A401) was indistinguishable from baseline performance by the 2nd month post-injury. The third monkey, A385, was much more variable, with sessions within the baseline range, interspersed with sessions with poorer than baseline performance. However, this monkey still successfully reached 46% to 86% of baseline performance on the "Difficult Task" over weeks 6 to 13. The association of grasping the handle to receive a reward was not substantially affected by CCI-injury as evidenced by the consistant performance on the "Easy Task".

This study is unique in demonstrating the feasibility of the CCI approach to modeling long-term recovery aftger TBI in an NHP. However, the study has two notable limitations: First, while the relatively lissencephalic brain of the squirrel monkey aids greatly in the neurophyiological identification of somatosensory and motor areas for targeting the injury, the mechanical stress differs from more gyrencephalic brains. It has been suggested that mechanical injuries in gyrencephalic brains result in more brain deformation, especially at the base of the sulci.[Vink 2018.] In the more lissencephalic squirrel monkey brain, the mechanical stress, and hence the injury extent was largely limited to the cortical grey matter at the surface (**Figure 3**). Second, the motor impairments in the current study were relatively mild and somewhat transient. However, an advantage of the CCI approach with programmable devices is that the impact parameters can be easily adjusted to suit the goals of the particular study. Alternatively,

the injury location can be varied. In our particular model, it was important to select specific parameters for CCI to limit damage to the DFL area of M1, sparing premotor cortex and parietal-frontal connections related to behavioral goals and attentional control of movement[43,44].

These results emphasize the precision of the CCI model to produce a focal injury to target specific cortical areas such as M1 or premotor hand areas as needed. Moving forward, the NHP model will allow us to address complex interactions between specialized corticospinal connectivity related to corticospinal and corticobulbar projections from various premotor cortices that remain intact after the injury[45-49]. Although there are many similarities between sensorimotor networks in rodent and primates, organization of primate motor systems reflect evolution of specialized visuo-motor adaptations to arboreal environments[37,50]. Advances in clinical application and development of neuroprosthetics and brain-machine-brain interface devices depend on advancing models of primate cortical organization.

5.0 **References**

1. Capizzi, A., Woo, J., & Verduzco-Gutierrez, M. (2020). Traumatic brain injury: An overview of epidemiology, pathophysiology, and medical management. *Medical Clinics*, *104*(2), 213-238.
2. Galgano, M., Toshkezi, G., Qiu, X., Russell, T., Chin, L., & Zhao, L. R. (2017). Traumatic brain injury: current treatment strategies and future endeavors. *Cell transplantation*, *26*(7), 1118-1130.

3. Stein, D. M., Feather, C. B., & Napolitano, L. M. (2017). Traumatic brain injury advances. *Critical care clinics*, *33*(1), 1-13.
4. O'Connor, W. T., Smyth, A., & Gilchrist, M. D. (2011). Animal models of traumatic brain injury: a critical evaluation. *Pharmacology & therapeutics*, *130*(2), 106-113.
5. Ma, X., Aravind, A., Pfister, B. J., Chandra, N., & Haorah, J. (2019). Animal models of traumatic brain injury and assessment of injury severity. *Molecular neurobiology*, *56*(8), 5332-5345.
6. Osier, N., & Dixon, C. E. (2017). Mini review of controlled cortical impact: a well-suited device for concussion research. *Brain sciences*, *7*(7), 88.
7. Murphy, M. D., Guggenmos, D. J., Bundy, D. T., & Nudo, R. J. (2016). Current challenges facing the translation of brain computer interfaces from preclinical trials to use in human patients. *Frontiers in cellular neuroscience*, *9*, 497.
8. Rizzolatti, G., & Luppino, G. (2001). The cortical motor system. *Neuron*, *31*(6), 889-901.
9. Courtine, G., Bunge, M. B., Fawcett, J. W., Grossman, R. G., Kaas, J. H., Lemon, R., ... & Rouiller, E. M. (2007). Can experiments in nonhuman primates expedite the translation of treatments for spinal cord injury in humans?. *Nature medicine*, *13*(5), 561-566.
10. Stepniewska, I., Preuss, T. M., & Kaas, J. H. (2007). Thalamic connections of the dorsal and ventral premotor areas in New World owl monkeys. *Neuroscience*, *147*(3), 727-745.

11. Kaas, J. H., & Stepniewska, I. (2016). Evolution of posterior parietal cortex and parietal-frontal networks for specific actions in primates. *Journal of Comparative Neurology*, *524*(3), 595-608.
12. Nudo, R. J. (2010). Stroke recovery in non-human primates: a comparative perspective. *Brain Repair After Stroke*, 67. . S. C. Cramer and R. J. Nudo. Cambridge, UK, Cambridge University Press: 67-76.
13. Carter, A. R., Patel, K. R., Astafiev, S. V., Snyder, A. Z., Rengachary, J., Strube, M. J., Pope, A., Shimony, J. S., Lang, C. E., Shulman, G. L. & Corbetta, M. (2012). Upstream dysfunction of somatomotor functional connectivity after corticospinal damage in stroke. *Neurorehabilitation and neural repair*, *26*(1), 7-19.
14. Tsintou, M., Dalamagkas, K., & Makris, N. (2020). Taking central nervous system regenerative therapies to the clinic: curing rodents versus nonhuman primates versus humans. *Neural Regeneration Research*, *15*(3), 425.
15. Guggenmos, D. J., Azin, M., Barbay, S., Mahnken, J. D., Dunham, C., Mohseni, P., & Nudo, R. J. (2013). Restoration of function after brain damage using a neural prosthesis. *Proceedings of the National Academy of Sciences*, *110*(52), 21177-21182.
16.
17. Nishibe, M., Barbay, S., Guggenmos, D., & Nudo, R. J. (2010). Reorganization of motor cortex after controlled cortical impact in rats and implications for functional recovery. *Journal of neurotrauma*, *27*(12), 2221-2232.Andrews, B. T., Barbay, S., Townsend, J., Detamore, M., Harris, J., Tuchek, C., & Nudo, R. J. (2020). Unrepaired

decompressive craniectomy worsens motor performance in a rat traumatic brain injury model. *Scientific Reports*, *10*(1), 1-8.

18. Nudo, R. J., & Milliken, G. W. (1996). Reorganization of movement representations in primary motor cortex following focal ischemic infarcts in adult squirrel monkeys. *Journal of neurophysiology*, *75*(5), 2144-2149.
19. Nudo, R. J., Wise, B. M., SiFuentes, F., & Milliken, G. W. (1996). Neural substrates for the effects of rehabilitative training on motor recovery after ischemic infarct. *Science*, *272*(5269), 1791-1794.
20. Friel, K. M., & Nudo, R. J. (1998). Recovery of motor function after focal cortical injury in primates: compensatory movement patterns used during rehabilitative training. *Somatosensory & motor research*, *15*(3), 173-189.
21. Plautz, E. J., Milliken, G. W., & Nudo, R. J. (2000). Effects of repetitive motor training on movement representations in adult squirrel monkeys: role of use versus learning. *Neurobiology of learning and memory*, *74*(1), 27-55.
22. Frost, S. B., Barbay, S., Friel, K. M., Plautz, E. J., & Nudo, R. J. (2003). Reorganization of remote cortical regions after ischemic brain injury: a potential substrate for stroke recovery. *Journal of neurophysiology*, *89*(6), 3205-3214.
23. Plautz, E. J., Barbay, S., Frost, S. B., Friel, K. M., Dancause, N., Zoubina, E. V., ... & Nudo, R. J. (2003). Post-infarct cortical plasticity and behavioral recovery using concurrent cortical stimulation and rehabilitative training: a feasibility study in primates. *Neurological research*, *25*(8), 801-810.
24. Dancause, N., Barbay, S., Frost, S. B., Plautz, E. J., Chen, D., Zoubina, E. V., ... & Nudo, R. J. (2005). Extensive cortical rewiring after brain injury. *Journal of Neuroscience*, *25*(44), 10167-10179.

25. Eisner-Janowicz, I., Barbay, S., Hoover, E., Stowe, A. M., Frost, S. B., Plautz, E. J., & Nudo, R. J. (2008). Early and late changes in the distal forelimb representation of the supplementary motor area after injury to frontal motor areas in the squirrel monkey. *Journal of neurophysiology*, *100*(3), 1498-1512.
26. Stowe, A. M., Plautz, E. J., Nguyen, P., Frost, S. B., Eisner-Janowicz, I., Barbay, S., ... & Nudo, R. J. (2008). Neuronal HIF-1α protein and VEGFR-2 immunoreactivity in functionally related motor areas following a focal M1 infarct. *Journal of Cerebral Blood Flow & Metabolism*, *28*(3), 612-620.
27. Barbay, S., Plautz, E. J., Zoubina, E., Frost, S. B., Cramer, S. C., & Nudo, R. J. (2015). Effects of postinfarct myelin-associated glycoprotein antibody treatment on motor recovery and motor map plasticity in squirrel monkeys. *Stroke*, *46*(6), 1620-1625.
28. Plautz, E. J., Barbay, S., Frost, S. B., Zoubina, E. V., Stowe, A. M., Dancause, N., ... & Nudo, R. J. (2016). Effects of subdural monopolar cortical stimulation paired with rehabilitative training on behavioral and neurophysiological recovery after cortical ischemic stroke in adult squirrel monkeys. *Neurorehabilitation and neural repair*, *30*(2), 159-172.
29. Gharbawie, O. A., Stepniewska, I., Burish, M. J., & Kaas, J. H. (2010). Thalamocortical connections of functional zones in posterior parietal cortex and frontal cortex motor regions in New World monkeys. *Cerebral Cortex*, *20*(10), 2391-2410.
30. Rouse, A. G., & Schieber, M. H. (2018). Condition-dependent neural dimensions progressively shift during reach to grasp. *Cell reports*, *25*(11), 3158-3168.

31. Bury, S. D., Plautz, E. J., Liu, W., Quaney, B. M., Luchies, C. W., Maletsky, R. A., & Nudo, R. J. (2009). A novel device to measure power grip forces in squirrel monkeys. *Journal of neuroscience methods*, *179*(2), 264-270.
32. King, C., Robinson, T., Dixon, C. E., Rao, G. R., Larnard, D., & Nemoto, C. E. M. (2010). Brain temperature profiles during epidural cooling with the ChillerPad in a monkey model of traumatic brain injury. *Journal of neurotrauma*, *27*(10), 1895-1903.
33. Mao, H., Yang, K. H., King, A. I., & Yang, K. (2010). Computational neurotrauma—design, simulation, and analysis of controlled cortical impact model. *Biomechanics and modeling in mechanobiology*, *9*(6), 763-772.
34. Nudo, R. J. (2013). Recovery after brain injury: mechanisms and principles. *Frontiers in human neuroscience*, *7*, 887.
35. Dancause, N., & Nudo, R. J. (2011). Shaping plasticity to enhance recovery after injury. In *Progress in brain research* (Vol. 192, pp. 273-295). Elsevier.
36. Nudo, R. J. (2007). Postinfarct cortical plasticity and behavioral recovery. *Stroke*, *38*(2), 840-845.
37. Wise, S. P. (2006). The ventral premotor cortex, corticospinal region C, and the origin of primates. *Cortex*, *42*(4), 521-524.
38. Hamadjida, A., Dea, M., Deffeyes, J., Quessy, S., & Dancause, N. (2016). Parallel cortical networks formed by modular organization of primary motor cortex outputs. *Current Biology*, *26*(13), 1737-1743

39. Dea, M., Hamadjida, A., Elgbeili, G., Quessy, S., & Dancause, N. (2016). Different patterns of cortical inputs to subregions of the primary motor cortex hand representation in Cebus apella. *Cerebral cortex*, *26*(4), 1747-1761.
40. Côté, S. L., Hamadjida, A., Quessy, S., & Dancause, N. (2017). Contrasting modulatory effects from the dorsal and ventral premotor cortex on primary motor cortex outputs. *Journal of Neuroscience*, *37*(24), 5960-5973.
41. McNeal, D. W., Darling, W. G., Ge, J., Stilwell-Morecraft, K. S., Solon, K. M., Hynes, S. M., ... & Morecraft, R. J. (2010). Selective long-term reorganization of the corticospinal projection from the supplementary motor cortex following recovery from lateral motor cortex injury. *Journal of Comparative Neurology*, *518*(5), 586-621.
42. Lang, C. E., & Schieber, M. H. (2003). Differential impairment of individuated finger movements in humans after damage to the motor cortex or the corticospinal tract. *Journal of neurophysiology*, *90*(2), 1160-1170.
43. Harding, I. H., Yücel, M., Harrison, B. J., Pantelis, C., & Breakspear, M. (2015). Effective connectivity within the frontoparietal control network differentiates cognitive control and working memory. *Neuroimage*, *106*, 144-153.
44. Rinne, P., Hassan, M., Fernandes, C., Han, E., Hennessy, E., Waldman, A., ... & Bentley, P. (2018). Motor dexterity and strength depend upon integrity of the attention-control system. *Proceedings of the National Academy of Sciences*, *115*(3), E536-E545.
45. Baker, S. N. (2011). The primate reticulospinal tract, hand function and functional recovery. *The Journal of physiology*, *589*(23), 5603-5612.

46. Baker, S. N., & Perez, M. A. (2017). Reticulospinal contributions to gross hand function after human spinal cord injury. *Journal of Neuroscience*, *37*(40), 9778-9784.
47. Darling, W. G., Ge, J., Stilwell-Morecraft, K. S., Rotella, D. L., Pizzimenti, M. A., & Morecraft, R. J. (2018). Hand motor recovery following extensive frontoparietal cortical injury is accompanied by upregulated corticoreticular projections in monkey. *Journal of Neuroscience*, *38*(28), 6323-6339.
48. Fregosi, M., Contestabile, A., Badoud, S., Borgognon, S., Cottet, J., Brunet, J. F., ... & Rouiller, E. M. (2018). Changes of motor corticobulbar projections following different lesion types affecting the central nervous system in adult macaque monkeys. *European Journal of Neuroscience*, *48*(4), 2050-2070.
49. Zaaimi, B., Dean, L. R., & Baker, S. N. (2018). Different contributions of primary motor cortex, reticular formation, and spinal cord to fractionated muscle activation. *Journal of Neurophysiology*, *119*(1), 235-250.
50. Touvykine, B., Elgbeili, G., Quessy, S., & Dancause, N. (2020). Interhemispheric modulations of motor outputs by the rostral and caudal forelimb areas in rats. *Journal of Neurophysiology*, *123*(4), 1355-1368.

Figure Legends

Figure 1 A - B. Motor skill assessment apparatus. A. Klüver Disk Task. This task was used to train and assess skilled use of grasping during a reach and retrieval task. Monkeys were required to retrieve a single 45 mg food pellet (3.56mm diameter) delivered singularly to five food-wells. Each food well was 5 mm deep and ranged in diameter from 9.5 mm to 25 mm. B. Hand Grip Task. This task was used to assess ability of monkeys to apply and sustain a power grip within a range of either 100 – 300 g of force for 3 seconds ("Difficult" task) or 20 – 500 grams of force for 0.5 seconds ("Easy" task).

Figure 2 A - C. Verification of lesion. A. Post-mortem photograph of the perfused brain of monkey A401 three months after a CCI injury. The CCI impact is seen within the red circle on the photograph. The blue circle indicates the position of the craniectomy made during the initial procedure to access cerebral cortex for identifying M1 and adjacent motor and somatosensory areas. Dark red areas in the photograph along the blue outline resulted from residual blood around perimeter of craniectomy that did not wash out during postmortem perfusion. B. Interaoperative photograph of the cerebral cortex within the cranial opening taken three months after CCI injury showing sites where neural recordings were acquired. Large red outline shows distortion of impacted cortex three months after CCI. Neural recordings were acquired from intact cortex adjacent to injury (large blue filled circles) and from infarct area (large black filled circles). Cutaneous responses were also obtained in primary somatosensory cortex. Topographical organization of the hand responsive to cutaneous stimulation was sampled in somatosensory cortex. The resulting cutaneous hand-map appeared normal

throughout areas 3a, 3b, and area 1 / 2. Sites where neural responses were evoked from cutaneous stimulation of the digits are shown as small red filled circles; glabrous cutaneous responses along the hand are shown as small white filled circles outlined in black. C. Neural spike recordings from inside impact area labeled “1” and outside impact area labeled “2”. Neural activity during a 1 second sample is shown for 16 channels acquired from depths of 200 to 1,700 μm (left side of each figure). Very little spontaneous spiking activity was observed within the impact area (Site 1) compared to an adjacent non-impacted site (Site 2), indicating that the lesion was effective throughout the depths of the grey matter.

Figure 3. A. Intraoperative photographs of exposed cortex before and after CCI. Solid red outline identifies target for CCI before impact in Pre-CCI column whereas a dashed red circle identifies the corresponding cortical surface (based on vascular patterns) three months after impact in Post-CCI column. B. Cortical area under impact was reduced by 85.6% (16.8 mm^2), 76.7% (15.1 mm^2) and 73. 57% (14.5 mm^2) in A413, A385 and A401, respectively. C. Coronal Sections (Weil stain). First column shows photos (2.5X) of coronal sections through the impacted area in each of the three monkeys. Second column is a magnified view of the location of impact. The Weil-stained sections were used to estimate area of the corona radiata underlying the area of cortical infarct.

Figure 4. Hand dexterity as assessed by the Klüver Disk Task. Motor performance (digit flexions) was determined relative to each monkey’s average pre-injury baseline distribution of scores over five sessions collected over a two-week period prior to CCI

injury. Following CCI injury, flexions per retrieval scores on a given weekly session (1 to 13) were converted to z-scores standardized to the mean and standard deviation of the individual monkey's baseline distribution. Scores falling outside of a 95% confidence interval (z=2.0) were considered significantly different from baseline. The 95% CI is designated by the grey shaded area. Scores outside of the shaded area are outside of the 95%. Weeks prior to CCI injury are indicated as negative numbers.

Figure 5. Hand grip performance. Number of successful grips on a given weekly session (1 to 13) was converted to z-scores standardized to the mean and standard deviation of the individual monkey's baseline distribution. The 95% CI for each monkey is designated by the grey shaded area. Scores falling outside of the shaded area (z=2.0) were considered significantly different from baseline. All monkeys were impaired to varying degrees on the "Difficult" task but only a mild transient deficit was observed on the "Easy" task.

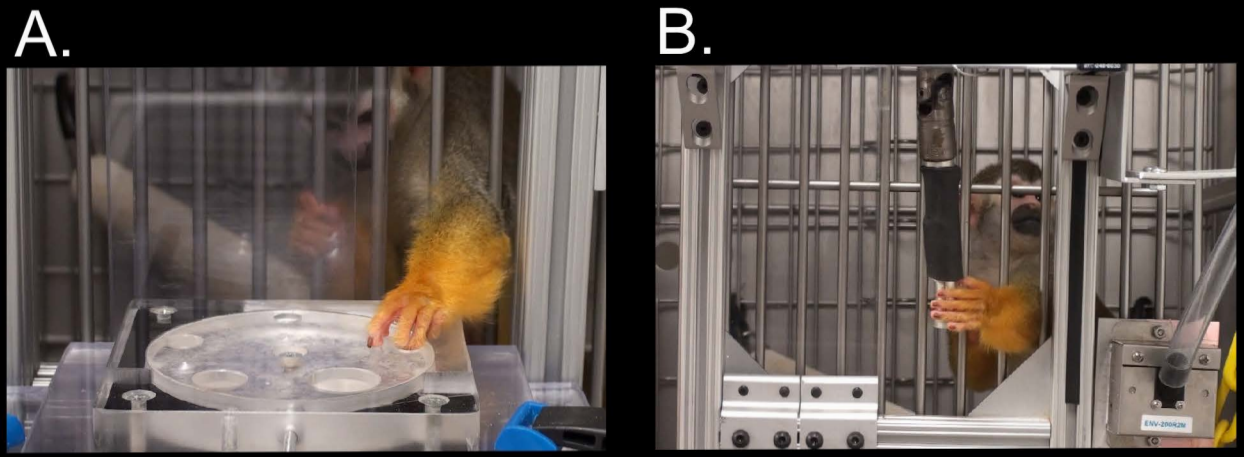

Figure 1

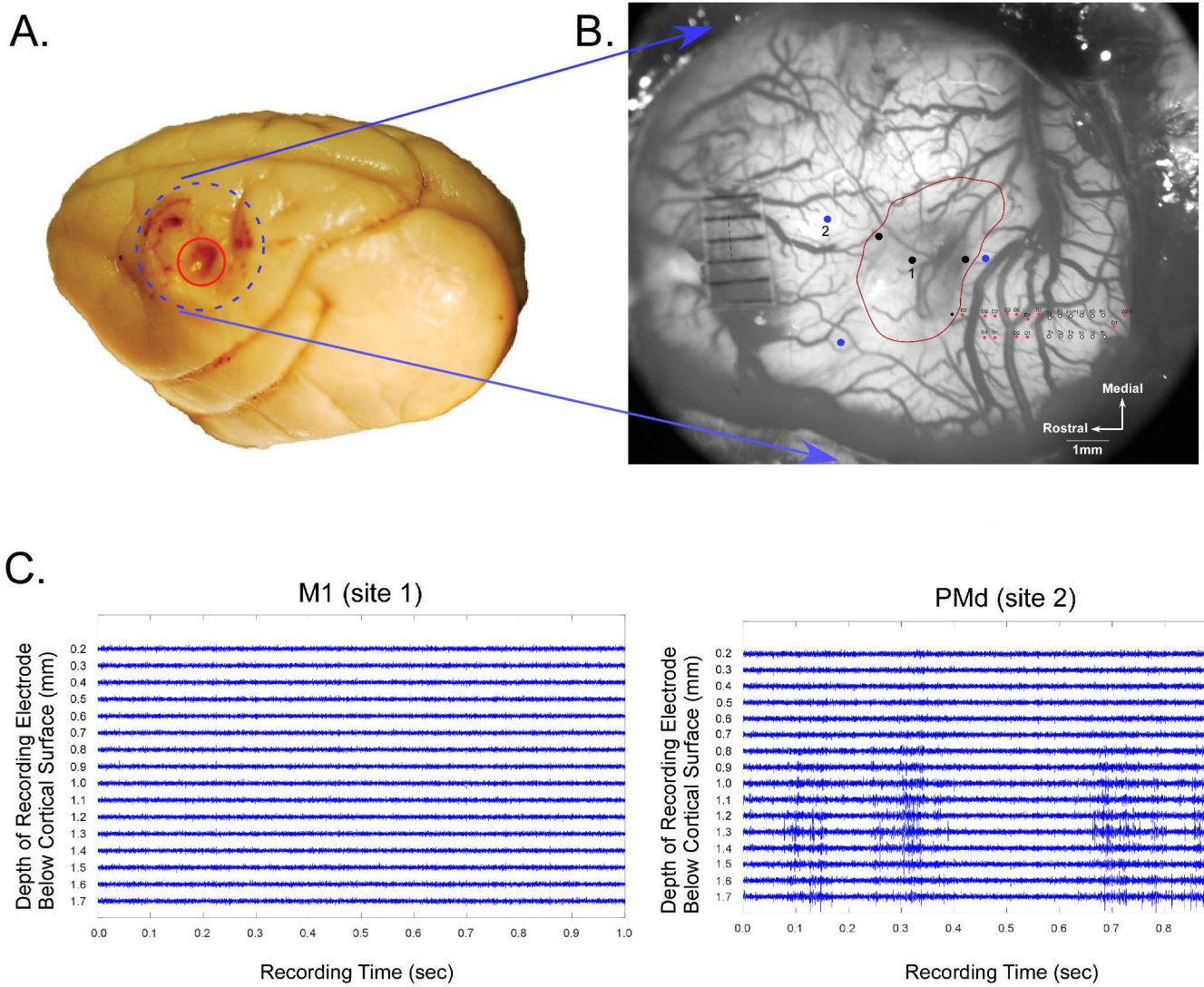
A.
B.
2
1
Medial
Rostral
1mm
C.
M1 (site 1)
PMd (site 2)
Depth of Recording Electrode Below Cortical Surface (mm)
0.2
0.3
0.4
0.5
0.6
0.7
0.8
0.9
1.0
1.1
1.2
1.3
1.4
1.5
1.6
1.7
0.0
0.1
0.2
0.3
0.4
0.5
0.6
0.7
0.8
0.9
1.0
Recording Time (sec)

Figure 2

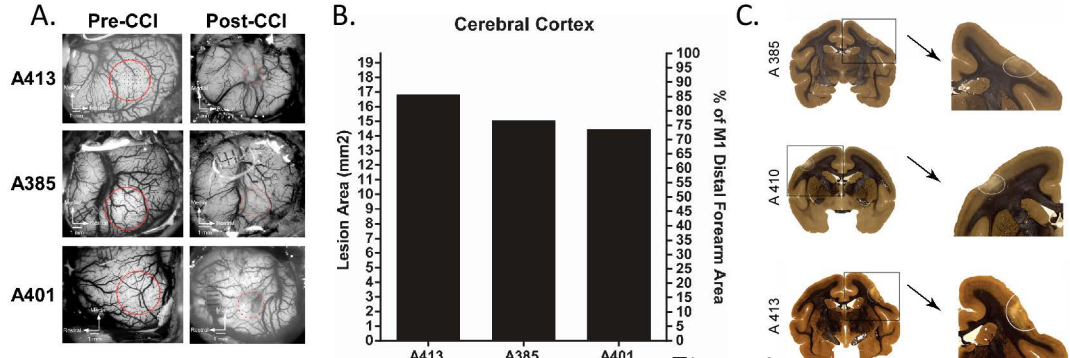
A.
Pre-CCI
Post-CCI
A413
A385
A401
B.
Cerebral Cortex
Lesion Area (mm2)
% of M1 Distal Forearm Area
A413
A385
A401
C.
A 385
A 410
A 413

Figure 3

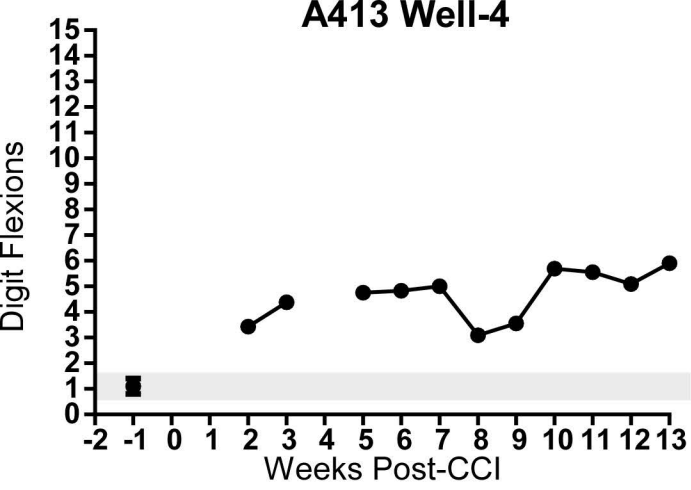
A413 Well-4
Digit Flexions
Weeks Post-CCI

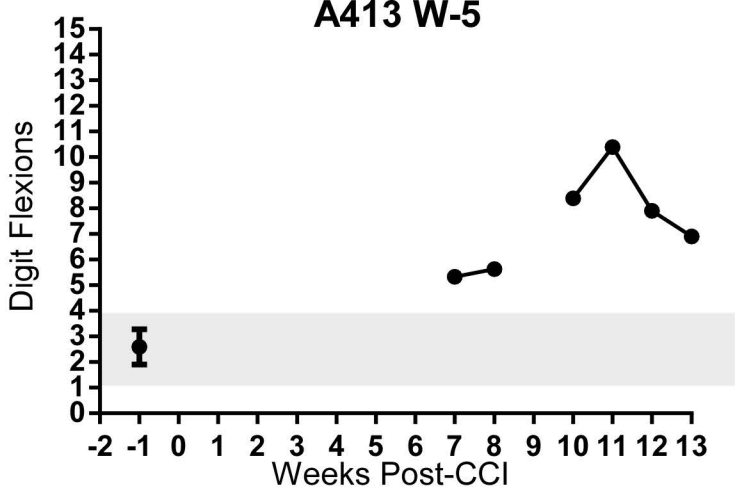
A413 W-5
Digit Flexions
Weeks Post-CCI

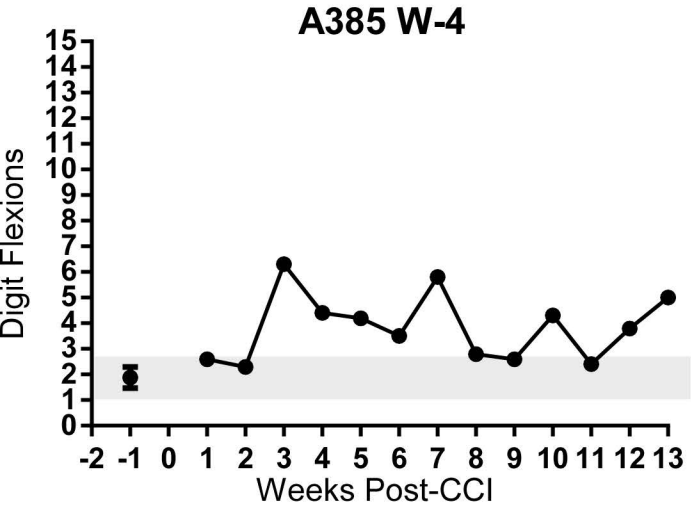
A385 W-4
Digit Flexions
Weeks Post-CCI

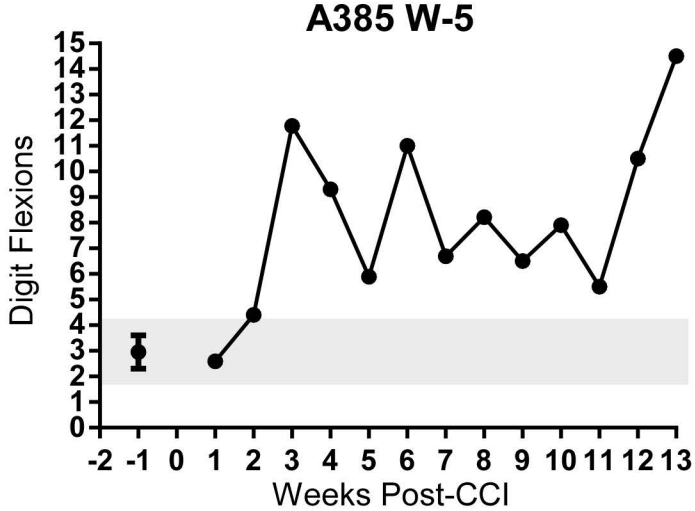
A385 W-5
Digit Flexions
Weeks Post-CCI

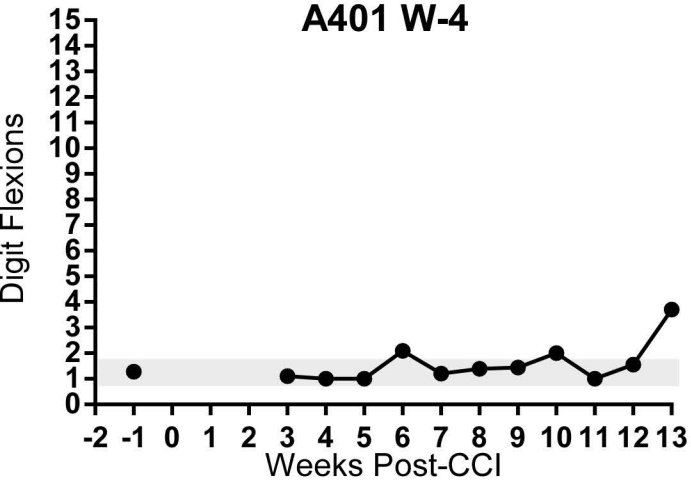
A401 W-4
Digit Flexions
Weeks Post-CCI

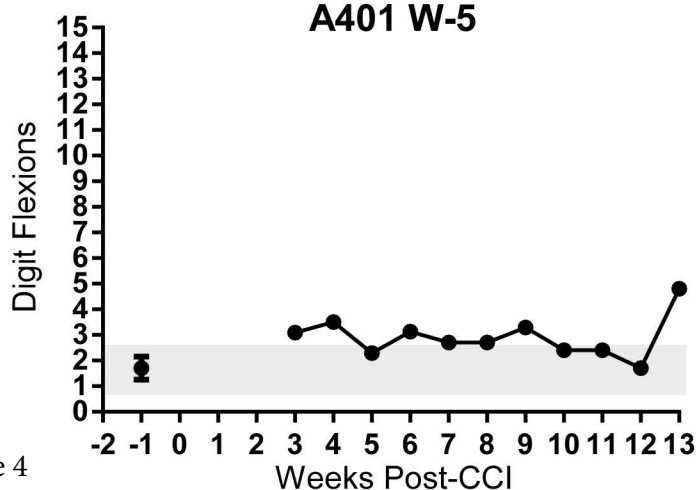
A401 W-5
Digit Flexions
Weeks Post-CCI

Figure 4

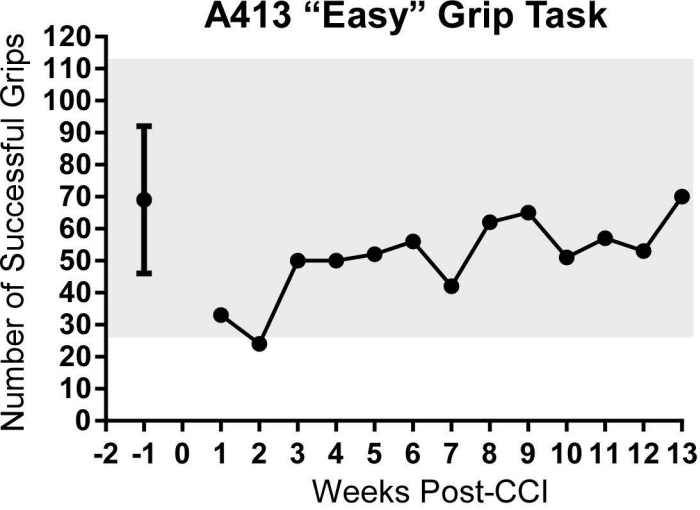
A413 "Easy" Grip Task
Number of Successful Grips
Weeks Post-CCI

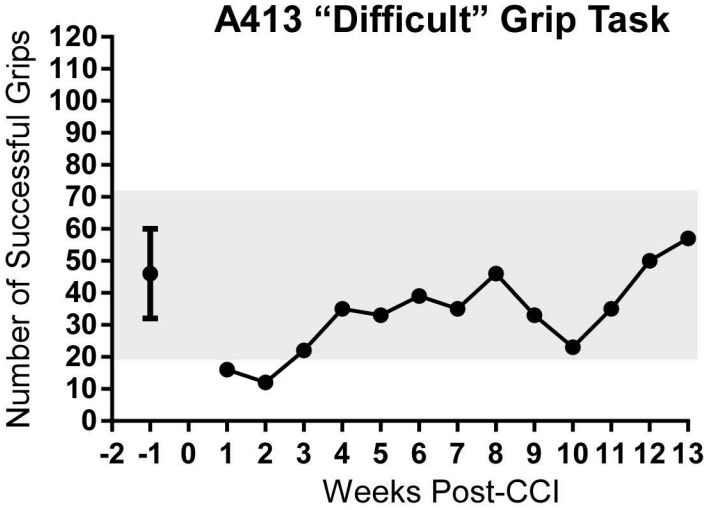
A413 "Difficult" Grip Task
Number of Successful Grips
Weeks Post-CCI

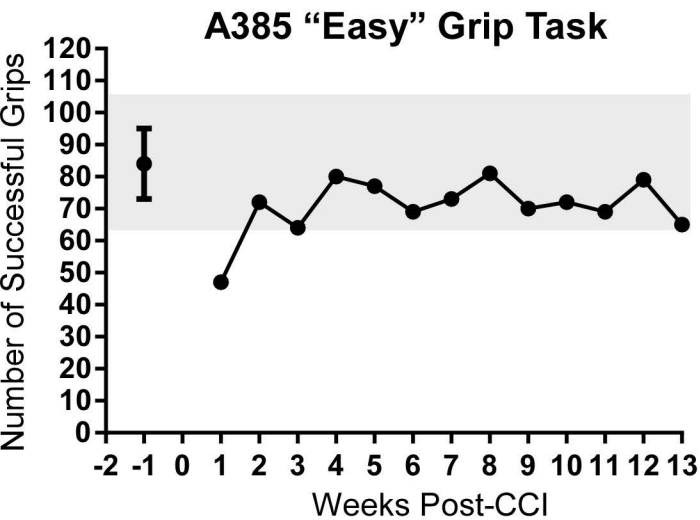
A385 "Easy" Grip Task
Number of Successful Grips
Weeks Post-CCI

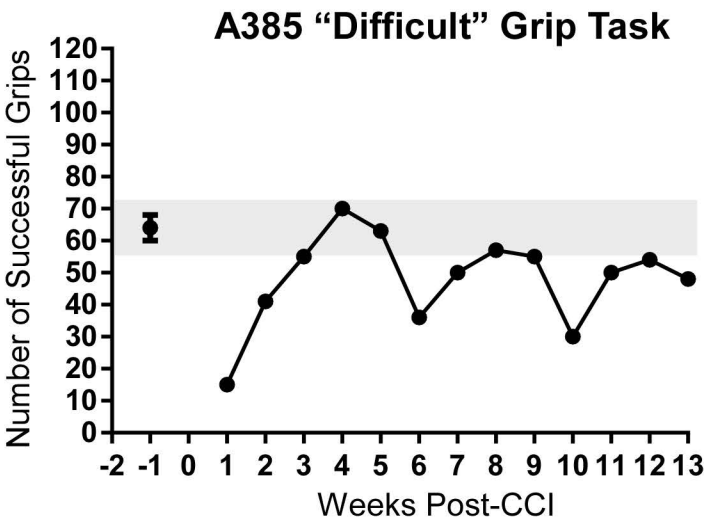
A385 "Difficult" Grip Task
Number of Successful Grips
Weeks Post-CCI

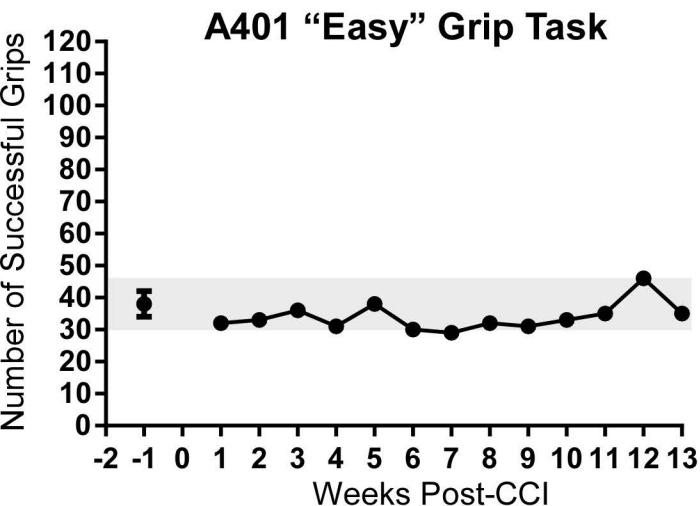
A401 "Easy" Grip Task
Number of Successful Grips
Weeks Post-CCI

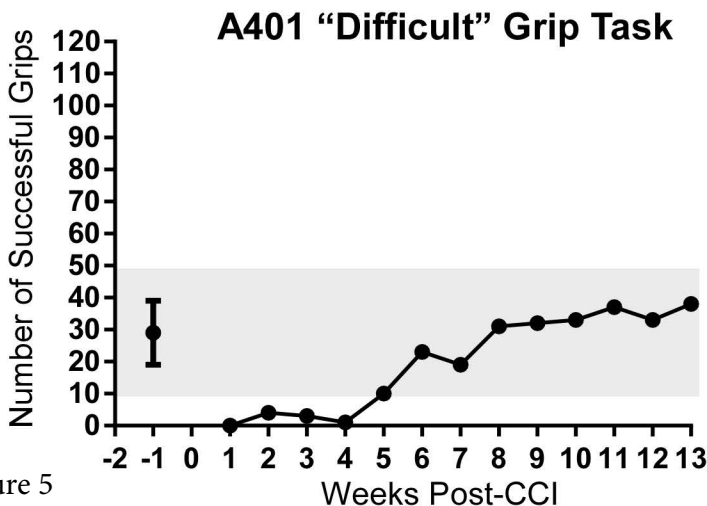
A401 "Difficult" Grip Task
Number of Successful Grips
Weeks Post-CCI

Figure 5